REPORT DOCUMENTATION PAGE

Public reporting burden for this collection of information is estimated to average 1 hour per response, including the time for reviewing instructions, searching existing data sources, gathering and maintaining the data needed, and completing and reviewing the collection of information. Send comments regarding this burden estimate or any other aspect of this collection of information, including suggestions for reducing this burden, to Washington Headquarters Services, Directorate for Information Operations and Reports, 1215 Jefferson Davis Highway, Suite 1204, Arlington, VA 22202-4302, and to the Office of Management and Budget, Paperwork Reduction Project (0704-0188), Washington, DC 20503.

1. AGENCY USE ONLY (Leave Blank)	2. REPORT DATE 21 NOV 1997	3. REPORT TYPE AND DATES COVERED Final Technical 7/1/96-6/30/97

4. TITLE AND SUBTITLE
Characterization of Seismic Sources Using Empirical Green's Functions

5. FUNDING NUMBERS
F49620-94-1-0273

6. AUTHORS
Shirley A. Rieven and William L. Rodi

AFRL-SR-BL-TR-98-

0187

7. PERFORMING ORGANIZATION NAME(S) AND ADDRESS(ES)
Earth Resources Laboratory
Dept. of Earth, Atmospheric, and Planetary Sciences
Massachusetts Institute of Technology
42 Carleton St., Cambridge, MA 02142

9. SPONSORING / MONITORING AGENCY NAME(S) AND ADDRESS(ES)
AFOSR/NL
110 Duncan Avenue, Suite B115
Bolling AFB, DC 20332-0001
Program Manager: Dr. Stanley K. Dickinson

10. SPONSORING / MONITORING AGENCY REPORT NUMBER

11. SUPPLEMENTARY NOTES

12a. DISTRIBUTION / AVAILABILITY STATEMENT
Approved for Public Release; Distribution Unlimited

12b. DISTRIBUTION CODE

13. ABSTRACT (Maximum 200 words)

Our work on the 1993 microearthquake swarm at the Larderello geothermal field suggests that the most significant obstacle to the practical application of correlation techniques, such as EGFs or relative event location for seismic events recorded at regional distances, is due to the degree of waveform complexity that is related solely to scattering effects along the path. In this study, we showed that despite similar focal mechanisms and a regional scale that is on the order of 1 to 2 wavelengths, the complexity of the waveforms was severe, particularly for S waves. We showed that the event waveform types exhibited at least two distinctly different characters, thus forcing the use of more than one master event. We show that the practical difficulties were partially mitigated by a very careful and detailed analysis of correlation coefficients between master and slave events and multiple pass culling of the rms residuals from the inversion results. This effort clearly reduces the efficiency with which these techniques can be applied to large clusters and presents some new challenges in developing practical algorithms. However, in the case of the Larderello 1993 cluster, we are encouraged that the final result so clearly agreed with known geologic structures. This suggests that refinements of the correlation techniques, in ways that reduce the effects of scattering, may further improve the results. One possible direction may be to introduce more thorough modeling of the scattered wavefield and removal of the nonessential phases from the waveform. This may improve the correlation coefficients by increasing the usable window length.

14. SUBJECT TERMS
Empirical Green's function, relative event location, Larderello

15. NUMBER OF PAGES
67

16. PRICE CODE

17. SECURITY CLASSIFICATION OF REPORT UNCLASSIFIED	18. SECURITY CLASSIFICATION OF THIS PAGE UNCLASSIFIED	19. SECURITY CLASSIFICATION OF ABSTRACT UNCLASSIFIED	20. LIMITATION OF ABSTRACT

NSN 7540-01-280-5500

19980223 115

Contents

0.1 INTRODUCTION

This is a final report for grant (F49620-93-1-0424) titled "Characterization of Seismic Sources Using Empirical Green's Functions" under the Parent Contract titled "Seismic Wave Radiation, Propagation and Event Location in Laterally Heterogeneous Media". The goal of this work was to investigate the use of the empirical Green's function method for seismic source characterization and discrimination in nuclear monitoring. The motivation underlying this investigation is to support the development of techniques capable of decomposing complex seismic events, detecting anomalous events, and discriminating underground nuclear explosions from other seismic events.

Seismic monitoring of the Comprehensive Test Ban Treaty (CTBT) entails using teleseismically and regionally recorded ground motions generated by a seismic source to estimate the location, focal mechanism, and time history of energy release of the source. These source parameters allow the discrimination between underground nuclear explosions and natural or other man-made events. The fundamental difficulty implicit in this task is that seismic data depend as much on the properties of the earth through which the energy has propagated as they do on the source parameters. Thus, seismologists attempt either to isolate features of seismic data that are relatively less sensitive to the propagation path, or to calibrate path effects empirically and with numerical models.

A potentially useful way to deal with this problem is to use the recordings from multiple sources to infer differences between their source parameters. That is, if two or more seismic events have sufficiently similar locations, the propagation effects to a given receiver will be similar and differences between the recorded seismograms will reflect, primarily, differences between the source parameters.

One method that adopts this approach is the empirical Green's function method for estimating the source time function of one event relative to another (Hartzell, 1978; Mueller, 1985). A second method is relative event location using differential arrival times between event pairs, as measured by the cross-correlation of waveforms (Poupinet *et al.*, 1984; Phillips

November 20, 1997 19:01

et al., 1992). M.I.T. has tested the usefulness of empirical Green's function and relative event location methods for locating and identifying events in the context of the CTBT in previous work supported by the Air Force (Toksöz *et al.*, 1993; Riviere-Barbier *et al.*, 1993; Rodi *et al.*, 1994; Li *et al.*, 1994, 1995, 1996).

The EGF method attributes waveform differences to variations in the source time functions of two events. Thus, as it is usually applied, it is required that the two sources be located close together so that none of the waveform differences are due to location or path effects.

In the relative event location method, it is assumed that seismograms from two closely spaced events will have a high degree of correlation, and that the lag of their cross correlation function, at a given receiver, reflects the difference between the traveltimes to the receiver. In fact, this will be the case only when the source time functions of the events are the same and when scattering near the source has the same effects on their seismograms. Waveform similarity between closely spaced events of similar mechanism is routinely observed, but the degree of similarity appears to degrade with event separation. Israelsson (1990) reported this to be the case for a cluster of industrial explosions he studied, while Riviere-Barbier and Grant (1991) employed this property of waveform correlation in a cluster-analysis approach to event discrimination . Results of Toksöz *et al.* (1991a) , who analyzed waveform similarity as a function of frequency and as a function of *receiver* separation (for a common earthquake source), suggest that scattering differences is the main reason why waveform similarity degrades with event separation. Therefore, one expects relative event location to become more difficult as the distance between events increases.

In an effort to develop seismological techniques that can be used to discern natural earthquakes from induced events at regional distances we can consider the application of either EGFs or relative event location methods. However, as we discussed above, the degree of correlation can be shown to decrease with increasing distance between events and is related to the degree of scattering along the path. The problem of obtaining correlations between waveforms that represent true variations in either location or source time function (rather than scattering effects) presents a significant challenge to the practical application of either

4   November 20, 1997 19:01

technique.

In the next section of this report, we present the results of the application of relative event location to a cluster of natural events as recorded by a regional seismic network in the Larderello Geothermal region in Western Italy. We will show the entire analysis of this cluster and interpret the results with respect to the known geology. Upon conclusion, we will review the results of the waveform correlation for this case study and identify where the practical limitations arose in using this particular correlation technique in a regional setting.

0.2 CASE STUDY: LARDERELLO, ITALY 1993
MICROEARTHQUAKE SWARM

On March 20, 1993, seismometers connected to the Larderello seismic network began record-
ing a series of microearthquakes near the Larderello geothermal field in western Tuscany,
Italy (Figure 0-1. ENEL (the Italian Electric Power Company) produced the initial esti-
mates of the hypocentral locations, the individual event origin times, and estimates of their
magnitudes (Figures 0-2 and 0-3) (ENEL-Unita Nazionale Geotermica, 1993). The Earth
Resources Laboratory (ERL) at the Massachusetts Institute of Technology (MIT) extended
the analysis of this cluster to accomplish three objectives; 1) to more precisely determine the
hypocentral locations using multiple relative event location techniques, such that the cluster
geometry and overall location might suggest the geologic conditions and structures causing
the cluster, 2) to determine focal mechanisms for a portion of the earthquakes to ascertain
the local state of stress and supplement the information from the relocation inversion, and
3) to interpret the results from 1 and 2 in light of available geologic and geophysical data.

0.2.1 The Method of Multiple Relative Event Location by Differential Travel Times

Applicability of the Method

The technique of locating earthquake hypocenters using multiple relative event techniques
improves upon traditional methods of single event hypocenter location by placing additional
constraints on the results of the inversion. The constraints, which are added to the inversion
in the form of differential travel times, supplement the usual P and S arrival times. The
incorporation of these additional constraints is suggested by the similarity of waveforms
between related events. The fundamental premise is that events with identical waveforms
must be collocated (or very nearly so) (Geller and Mueller, 1980; Poupinet *et al.*, 1984; Ito,
1985; Thornjarnardottir and Pechmann, 1987; Ito, 1990; Israelsson, 1990; Pechmann and

Thorbjarnardottir, 1990; Deichmann and Garcia-Fernandez, 1992). We can use this similarity to improve the estimates of event source parameters (i.e. hypocenter coordinates and origin times) if we can identify and compensate for events whose waveforms are dissimilar. To do this we must first consider the cause of waveform variations.

Fremont and Malone (1987) state that variations in waveforms can be attributed to four main causes; fluctuations in the source time functions, changes in focal mechanisms, changes in the properties of the media, and changes in hypocentral location. In order to use waveform similarity to improve the locations, the method of differential travel times requires that the set of seismic events to be located are related to each other in both spatial and temporal aspects. Placing this constraint on the events controls, to a degree, one of the possible sources of waveform variation, specifically variations introduced by changes in the media properties. This is reasonable because if the temporal distribution of events is small, we can assume that the properties of the media have not changed significantly, and if the spatial distribution is also small then the changes in the travel times introduced by variations in velocity structure is minimized as well (Fremont and Malone, 1987).

The second possible cause of waveform variation that can be determined, if not controlled, is the focal mechanisms of the events. Fremont and Malone (1987) suggest that variations in focal mechanisms usually affects the waveform shape more than the arrival times of the P and S waves and therefore, do not constitute as strong a constraint as those imposed by the spatial and temporal correlations. In our study, we will show that the focal mechanisms for the Larderello cluster exhibit a high degree of similarity and therefore, no degradation of the waveform is expected from this variation source.

If the events in the cluster exhibit similar waveforms, then we can use cross-correlation techniques to determine the degree of similarity between them, and then either eliminate outliers completely or weight them appropriately in the relative location inversion. By identifying and controlling variations from other sources, we maximize the likelihood that any remaining variations are attributable only to changes in hypocenter coordinates.

Interest in the occurrence of events showing identical or nearly identical waveforms has increased in recent years as high precision location techniques are developed. Multiple events with a strong similarity in waveform have been classified into "families" or termed doublets, triplets or multiplets according to the number of similar events observed (Geller and Mueller, 1980; Frankel, 1982; Poupinet *et al.*, 1984; Fremont and Malone, 1987). An earthquake cluster exhibiting these characteristics is an excellent candidate for relocation using differential travel time techniques.

The Relocation Procedure

The location of source parameters by the method of differential travel times uses least squares inversion to iteratively solve the system of equationS $t_i - F_i = e_i$, where t_i is the observed travel time to the ith station, F_i is the calculated travel time to the ith station, and e_i is the observational error in t_i (Flinn, 1965; Jordan and Sverdrup, 1981; Menke, 1989).

The multiple event relocation method used here solves a non-linear system which is of the form:

$$d = A(h) + Bt + n \tag{0.1}$$

where; the data vector d contains the absolute and differential arrival times for a set of events, stations and phases, the model vector h contains the hypocenter coordinates of the events, the t vector contains the origin times of the events, and the vector n contains all errors attributable to observation irregularities and approximations in the estimate of the seismic velocity model. "A" is a nonlinear operator obtained from the function that determines the travel time of a seismic ray (based upon an estimate of the velocity structure, the estimated hypocenter locations and the location of the recording stations). B is a linear operator derived from the differential origin times of a slave event relative to the origin time of a master event . A and B are implicitly defined by models of the absolute or differential

8

arrival times.

For absolute arrival times our model is:

$$T_{esw} = t_e + F(x_e, x_s, U_w) + n_{esw}^{obs} \qquad (0.2)$$

and for differential arrival time referred to one master event we use

$$\delta T_{resw} = t_e + F(x_e, x_s, U_w) + n_{esw}^{obs} \qquad (0.3)$$

where the following definitions apply:

- subscripts e, s and w refer to event, station and wave type, respectively

- δT_{resw} refers to differential travel times for event e and wave w at station s referred to a reference event r

- t_e and t_r refer to the origin times of a particular event and reference event, respectively

- x_i is a vector containing the hypocenter coordinates

- U_w is the spatial dependence of the seismic slowness (reciprocal of velocity)

- $F(x_e, x_s, U_w)$ is the function defining the travel time of a seismic ray from the hypocentral coordinates of event e to the station s as determined from the seismic slowness function (a function of position)

- n_{esw}^{obs} is the observational error as it pertains to event e, station s, and wave w.

An additional source of error exists in that the slowness function is approximated by a one-dimensional model. This approximation affects the absolute relocations, but has been shown to have limited effects on the relative relocation of events whose true locations are separated by less than one wavelength (Rodi et al., 1993).

Estimates of the source parameters (the h and t vectors in equation (0.1) are found by minimizing the misfit between the observed and calculated travel times by using the Polak-Ribiere variant of the conjugate gradient method (Rodi et al., 1993).

November 20, 1997 19:01

The differential times are determined by calculating the degree of similarity between a master and slave event by cross-covariance and equivalently, cross-correlation techniques. Given two time series x and y, the cross-covariance function is defined as:

$$S_{xy}(x) = \int_{t_i}^{t_2-t_1} x(t')y(t'-t)dt \qquad (0.4)$$

and the cross-correlation function (the normalized form of the cross-covariance function) is:

$$C_{xy}(t) = \frac{S_{xy}(t)}{\sqrt{S_{xx}(0)S_{yy}(0)}} \qquad (0.5)$$

If the two events to be correlated are identical, equation (0.5) becomes the auto- covariance function. The differential times are determined by measuring the difference between the maximum peak of the cross-covariance function and the maximum peak of the auto- covariance function. The resulting differential times give the errors in the picks of the arrival for the slave events relative to the master events. The differential travel times were determined directly from the cross-covariances, where as the correlation coefficients were determined from the cross-correlation function, as defined.

0.2.2 The Method used to Determine Microearthquake Focal Mechanisms

Focal mechanisms for the Larderello microearthquakes were determined using a computer algorithm developed by Stewart Guinn and L.T. Long (1977). This algorithm uses forward modelling to predict the polarity, or "sense" of the first motion P wave arrivals for a set of seismic stations. The first motions are calculated based upon P wave radiation patterns from a dislocation source on a fault plane with known strike, dip and rake. Valid solutions include all fault planes that produce a match between the calculated first motions and the observed ones (Hermann, 1975; Guinn and Long, 1977).

The fault planes are determined by conducting a systematic search of all possible orientations of the local stress ellipse, which is related to the orientation of the fault plane through its normal and slip vectors (Aki and Richards, 1980). The search begins by orienting the null stress axis (the B axis) in the vertical direction and then rotating the compressional and tensional axes (P and T, respectively) around the B axes at a preset angle of rotation. The algorithm then calculates the strike and dip of the two nodal planes and two rakes associated with each orientation of the stress ellipse, and based on these, predicts the "sense" of the P wave first motions at each station. In order to accommodate the potential for incorrect first motion determinations, the user may specify the conditions under which a solution is accepted by allowing a set number of inconsistent first motions in the solution set. The final output consists of the azimuth and plunge of each axis and the strike, dip and rake for each nodal plane that produces a match (Guinn and Long, 1977).

All solutions which match the observed data are recorded as equally valid solutions with three "axis domains" defined. For well constrained problems, the domains are small. For example, if 50 solutions are found that match the data, a well constrained solution set will have all 50 B axes located within a small area, and likewise for the other axes. If the solution set is poorly- constrained then the axis domains will define large and perhaps convoluted shapes (Guinn and Long, 1977).

0.2.3 Results

The 1993 Larderello microearthquake cluster is an appropriate choice for the application of multiple event relocation using differential travel times because it meets the criteria discussed earlier. The cluster occurred in a spatially restricted zone near the northern boundary of the Larderello geothermal region. Although the initial hypocentral locations suggested diffuse seismicity over a volume of approximately 5 cubic kilometers, an evaluation of the waveforms indicated a high degree of similarity, suggesting that the true locations are more closely located than that suggested by the single event inversion. Temporally, the cluster occurred over the course of a few days, with origin time intervals ranging from minutes to

hours (See Figure 0-3). The distribution of magnitudes, in combination with waveform similarity, suggests that the events can be classified into multiplets, which supports the use of cross-correlation techniques.

The cluster was recorded by the Larderello seismic network which is a local array of thirty-one short period seismometers. ENEL provided MIT with seismic records of 200 events recorded by twenty-one of the thirty-one stations. Nineteen of these stations were equipped with seismometers that recorded the vertical component of ground motion only. The remaining two stations recorded all three components, i.e. north, east and vertical.

The events included in this study were chosen such that there was a high percentage of stations actively recording during that time period. In addition, 100 consecutive events were chosen rather than 100 randomly distributed ones. This was done so that if it was later discovered that a high degree of correlation existed between the temporal and spatial distribution of events, then the variation in velocity structure between consecutive events would be as small as possible, improving the likelihood that the waveform correlation would be high as well.

Relocation of the Larderello cluster was accomplished in three phases beginning with the determination of the absolute and differential times, followed by inversion for event source parameters (i.e. hypocentral locations and origin times), and finally calculation of focal mechanisms. The following discusion outlines the methods used, detail the results, and present an interpretation in light of other geologic and geophysical data.

Determining differential travel times for the Larderello earthquakes was completed in seven stages:

- P and S phase picking

- Identifying multiplets

- Determining P and S window lengths and filtering parameters

- Choosing master events

- Choosing stations to be included in the inversion

- Performing the cross-correlations

P and S arrival times were identified and marked in the headers of 86 events recorded at 21 stations. The sense of the P wave first arrival was also recorded, in anticipation of the determination of focal mechanisms. Figure 0-4 presents records from one station. The sampling interval for all records was 0.004 seconds. Preliminary estimates of 0.02 and 0.04 seconds were assigned for the standard deviation of the P and S arrival time picks (referred to as 'absolute' arrival times).

During the P and S phase picking, two characteristic waveforms were identified. These waveforms were designated as Types I and II and appear to be characteristic of two multiplets occurring within the larger cluster. Referring to Figure 0-4, note that events 147 and 148 are similar and of Type II and Events 149 and 150 are similar and of Type I. Event 184 is also of Type II, but the similarity is less pronounced than for the others. (The numerical designation indicates the relative order in origin times of the events). The waveforms for events 147 and 148 are similar in their full length, as are the records from events 149 and 150. The magnitudes of these events are not identical in the pairs, but are similar (e.g. 1.14 vrs. 1.34 for events 149 and 150, respectively). Despite variations in magnitude, the similarities in waveform persist, and we note that in general, the events which could be classified as either Type I or II were found to have a magnitude between 0.76 and 1.55. Figures 0-5 and 0-6 show the cross-covariances of these event records with an event of each type (II and I, respectively). These cluster characteristics are similar to those found by other research groups investigating multiplets from other earthquake clusters (Fremont and Malone, 1987; Pechmann and Thorbjarnardottir, 1990; Deichmann and Garcia-Fernandez, 1992).

Window lengths for the P and S phases were determined for each station by estimating the maximum possible time duration that would exclude any portion of a later arrival. For

November 20, 1997 19:01

example, the window length for Type II events, such as 147 (Figure 0-4) needed to have an offset less than 0.35 seconds after the P arrival in order to exclude the second arrival. The full length of the windows are a compromise between the need to exclude these later arrivals and the need to include enough cycles of the desired arrival to make the correlations valid. In addition, the actual window lengths for each station and phase were determined based upon an evaluation of the amplitude spectra for events recorded at the station. In all cases, the window lengths were between 0.5 and 0.8 seconds long depending upon the station. Figure 0-7 shows an example of an event's amplitude spectrum at station CORN. The majority of spectral energy falls between 5 and 15 Hertz with a marked increase between 8 and 13 Hertz. Window lengths of 0.5 seconds allow four cycles of an 8 Hertz wave. Longer window lengths were used whenever the records for a station indicated the absence of a second arrival within that interval, so that the lower frequencies would be represented in the correlation. Prior to performing the correlations, the full waveforms were bandpass filtered (corners of 5 and 20 Hertz) and a cosine taper was applied to the window.

Master events were selected on the basis of clarity and impulsiveness of P and S arrivals, low noise and good coverage by stations (i.e. masters recorded at as many stations as possible). Several attempts were made to use only two masters for the entire cluster of events, however, an unacceptable proportion of low correlations required the use of multiple masters. So, the cluster was divided into four subsets, each with 2 masters, one of each type. For example, events 150 and 156 were used as masters for events 141 through 156. For events 116 through 140, a strong type II master was not identified, thus, event 126 was included as a secondary master for that group. Figures 0-8 and 0-9 present the master events at station POMA.

Stations used in the inversion exhibited the following characteristics; most of the master events and many of the regular events were recorded, and the signal-to-noise ratio was acceptable. Additionally, distance and azimuthal coverage were also used as criteria. The stations that were excluded exhibited poor signal-to-noise ratios or recorded only a limited number of events. The final stations chosen were: CLSV, CORN, FRAS, MINI, MONV, POMA and SCAP (See Figure 0-2).

Differential travel times for each phase (P and S) were determined for each of the 86 events at each of the stations. The following master-slave event pairs were used; events 126 and 131 were masters for events 116-140, events 150 and 156 were masters for events 141-156, events 171 and 186 were masters for events 157-187 and events 189 and 191 were masters for events 188-218.

Differential travel times were calculated for each phase using the following equation:

$$dt = tt_{master} - tt_{slave} - \epsilon_{picking} - \epsilon_{waveform} \qquad (0.6)$$

where,

$$tt_{master} = at_{master} - T0_{master}$$

$$tt_{slave} = at_{slave} - T0_{slave}$$

In practice, the use of the origin times is avoided by introducing a common reference time for both events and normalizing the arrival times to the master events arrival times.

Figure 0-11 shows a schematic diagram of the elements of the differential time. For ease of illustration, we choose to demonstrate the process of determining differential times using a master and slave pair that are coincident in time (as indicated in the figure by their coincident origin times, T0). The master event arrival times show a unique moveout curve for any particular array of stations. (The array we are using here is a linear array which we choose for convenience in order to show a simply shaped moveout curve). The slave event arrival time moveout curve exhibits a slightly different shape, which is an expression of the difference in location between the master and the slave events. When the two events are identical in all ways except location and we declare (for this example) that the picking error is zero, then the epsilons in equation (0.6) are zero and we can derive the differential times directly from the absolute time picks. Usually, however, picking error is not negligible and there are some variations in the waveform due to the change in location. We assume that there are no variations in focal mechanism and source time functions and

15   November 20, 1997 19:01

so all waveform variations are due to changes in hypocenter location only. If the events are sufficiently close together then the waveform variations will be small and we can use correlation techniques to remove any temporal offsets (epsilons) caused by the slight waveform differences. Additionally, the correlation will also remove any picking inconsistencies by using the pick on the master event (per station) as a reference. It will not, however, remove picking inconsistencies between stations.

The temporal offsets (also refered to as correlation offsets) were determined by cross-covariance of a P or S window from a slave event and a corresponding P and S window from a master event. Figures 0-10 through 1 0-14 illustrate the determination of the offsets from the cross-covariances. The time lag between the cross-covariance peak and the auto-covariance peak is the correlation offset.

The correlation offsets, taken as a set of data, are expected to exhibit the statistical characteristics of a gaussian distribution with zero mean and variance (Jordan and Sverdrup, 1981; Rodi *et al.*, 1993) Figures 0-15 and 0-16 present examples of the distributions of cross- correlation offsets for P and S waves for the 86 events from the Larderello cluster (as recorded at station POMA). The distribution of the P wave offsets clearly shows the expected characteristics, while the distribution of the S wave offsets suggest that the original S wave arrival time picks were affected by a non-random influence. This influence is most likely related to the masking of the S wave first arrivals by P wave coda and P-to-S or S-to-P conversions. For some of the stations and events, earlier arrivals were superimposed on the S wave first arrivals making them difficult to pick. For those stations and events, the expected S wave arrival times were anticipated based upon a set of clear arrivals and three-component records (when available). These reference S waves were associated with a particular peak in the waveform and then traced through the rest of the records. This technique would maximize the likelihood that the true S arrival would occur within the chosen window, allowing the cross-correlation to detect it, but the bias would then appear as a non-random effect in the distribution of the correlation offsets.

The standard deviations of the P and S differential travel times were estimated by taking, as

a baseline, values of 0.004 seconds for the P waves and 0.008 seconds for the S waves. These values were then modified for each master-slave pair by dividing by the cross-correlation coefficient, so that pairs showing the highest degree of correlation would have the smallest possible standard deviations.

Depth Below sea level	P Wave velocity (m/s)	S Wave velocity (m/s)
0	3,500	2,000
300	5,500	3,200
3,000	6,000	3,500

Table 0.1: 1-D velocity structure model (version 0).

Hypocenter Inversion

The multiple relative location inversion involved two steps:

- Developing starting models for the hypocenters and 1-D velocity structures

- Inverting for the full set of locations, evaluating the results and estimating errors

- Evaluating errors

The starting model for the hypocenter locations was based upon ENEL's initial hypocenter estimates from the single event inversion. All events were assigned the same guess of 25,000 meters north of the local coordinate system origin and 33,000 meters east of the origin. This starting model would eventually be modified several times to reflect the results from subsequent inversion trials. Several different velocity models were used in the inversion. These models evolved as additional information became available regarding known geological characteristics of the region. The development and evolution of these models was based on available geological information which will be discussed in detail in a later section of this paper (Tables (0.1), (0.2), and (0.3).

The hypocenters and origin times were determined using the non-linear, conjugate gradient inversion algorithm described earlier. Various starting models were tried until the best fit to the observed data were obtained. The final results were found using a starting model of 25,000 m north, 35,000 m east and 4600 m depth and version 2 of the velocity model (0.3).

Depth Below sea level	P Wave velocity (m/s)	S Wave velocity (m/s)
0	3,500	2,000
500	4,800	2,700
1,000	5,900	3,200
4,800	4,900	2,800

Table 0.2: 1-D velocity structure model (version 1).

Depth Below sea level	P Wave velocity (m/s)	S Wave velocity (m/s)
0	4,500	2,360
400	4,800	2,800
500	5,900	3,200
3,000	6,100	3,500
4,000	4,900	2,865
4,200	6,100	3,500

Table 0.3: 1-D velocity structure model (version 2).

Locations are shown in Figures 0-17 through 0-20, and the distribution of the residuals for the relative travel times are presented in Figure 0-21.

To evaluate the results in terms of geometrical patterns we must consider two possible sources of bias; 1) hypocenters with large residuals, and 2) offsets in the locations of a subset relative to another subset due to the use of multiple masters.

Scatter introduced by poorly fit locations was eliminated by culling outliers on the basis of residual travel times, data standard deviation estimates and error ellipses from the inversion. All events whose travel time residuals exceeded three times the standard deviations of the data were excluded from the geometry analysis. This is a stricter criteria than using the standard deviations of the residuals and was chosen so that only the best fit data was used in the geometry analysis.

Errors due to multiple masters exist in the set of locations because the constraint placed on the inversion by the differential travel times between master-master pairs was relatively weak. Any geometric pattern in the locations may therefore be obscured by errors in the relative locations between subsets. It is necessary then, to eliminate the effects of these errors by separating the subsets and viewing them inpendendently. For each subset, one master was used as the dominant reference event because it was observed that one or the other of the masters produced higher correlations. Separating on the basis of masters ensures that master related scatter is removed. The separated and culled results are presented in Figures 0-22 through 0-25.

Two of the subsets (events 157-187 and 188-218) show distinct lineations. The two-dimensional confidence regions (for epicentral locations) and confidence intervals (for depth) give an indication of the likelihood of the apparent patterns. Figures 0-26 through 0-29 present some typical estimated confidence regions for the subsets of interest.

The absolute locations have been estimated from the master events, for example, the absolute location of event 191 is 25,808 m north, 35,033 m east and 5,070 m in depth. The uncertainties in absolute location for this event are 625 m (semi-major axis), 503 m (semi-minor axis), and 1,049 m in depth.

The pattern and shape of the error ellipses, as determined by the relative event locations for subset number 4 (events 188-218), indicate that the apparent lineation is not an artifact of uncertainties in the inversion results. Event 157-187 exhibit greater uncertainty in their locations, however, the common overlap of the elipses defines a very small region. It is unlikely that the northwest-southeast trend of the event locations can be reasonably attributed to this uncertainty. In light of this, the orientation of these two lineations should be compared with the the known geological structures and any other possible site specific associations. Patterns in relative depth distribution, however, are not well resolved, and therefore, any conclusions regarding depth should be derived from the absolute locations.

Focal Mechanisms

Focal mechanisms were determined for 17 events in the Larderello microearthquake cluster using first motion P wave data. The clarity of the P wave arrivals was excellent at most stations and no problems were encountered discerning the sense of the motion, as evidenced in Figures 0-8, 0-9, and 0-10. Several stations exhibited variations in the direction of motion indicating that rays from these stations were emerging near the nodal planes. These stations provided critical information and additional constraint on the final fault plane solutions. The solutions for the 17 events indicated little variation between mechanisms. Figure 0-30 represents examples of the extreme cases observed. An effort was made to use as many stations as possible and select events with the best coverage available, however, the azimuthal and distance coverage was impacted by a lack of stations in the northwestern quadrant and the location of the swarm near the northern boundary of the network. Events for which focal mechanisms could be determined were recorded by between 13 and 16 stations, generally including CLSV, CORN, CRBE, FRAS, FROS, LAGO, LURI, MBAM, MDSV, MGUI, MINI, MONV, POMA, SCAP, TRAV, VALE, and MLUC (Figure 0-17).

The number of valid solutions identified for each of the events varied according to how many stations were available and the particular set of first motions, however, all events exhibited well defined domains for the three principle axes of the stress tensor. Focal mechanisms were calculated using a search increment of 10 degrees, as recommended by Guinn and Long, and the number of inconsistent first motions was limited to one or zero (Guinn and Long, 1977). Solutions for all events indicate reverse faulting mechanisms ranging from nearly pure reverse to predominantly reverse with some strike-slip component. Average solution parameters for two representative events are listed in Tables (0.4) and (0.5).

	P Axis		T Axis		B Axis	
Event	Azimuth	Plunge	Azimuth	Plunge	Azimuth	Plunge
200	221	86	128	51	315	40
187	61	74	196	23	325	75

Table 0.4: Principle axes of stress for events 200 and 187.

	Event	Strike	Dip	Rake
NE Dipping	200	168	66	147
Nodal Plane	187	173	32	12
SW Dipping	200	272	61	28
Nodal Plane	187	319	63	73

Table 0.5: Strike, dip and rake of nodal plane for events 200 and 187.

0.2.4 Interpretation

Geologic Setting

The Tuscany region of Italy is associated with the Tyrrhenian-Apennine orogenic system which trends northwest through the Italian peninsula and marks the location of a sharply curved thrust belt that extends south and then west through Calabria and Sicily. Structures within this region reflect at least three separate phases of tectonic disturbances, which are recognized by remnant features in both the sedimentary formations as well as in some of the basement units. The primary structures of the Apennines formed during the Apennine Orogeny (middle-Apline Orogeny, middle Eocene to Oligocene, 30-50 ma) (Carmignani and Kligfield, 1990; Cameli *et al.*, 1993).

The first disturbance, the Eocene-Oligocene phase of deformations, is referred to by Carmignani and Kligfield (1990) as the D1 phase and is represented by structural features created by northeast-southwest oriented compression during the initial collision of the Corsica-Sardinia microplate with the Adriatic microplate . The D1 phase created nappe structures by displacing preexisting sedimentary formations along detachment horizons (Carmignani and

November 20, 1997 19:01

Kligfield, 1990).

The sedimentary formations involved in the nappe building are identified as the Ligurid complex and the Tuscan Nappe. The Ligurid complex is composed of Jurassic to Paleogene sediments, specifically flysch, pelagic sediments, radiolarites and ophiolites. The Tuscan nappe are composed of Triassic to Paleogene flysch, radiolarites, marls, limestones and anhydrites. These two units are overlain by neogene sediments (Cameli *et al.*, 1993; Batini *et al.*, 1985a).

The allocthonous Tuscan nappe is discontinuous due to extensional thinning and in some locations, is underlain or replaced by overthrust wedges of the autochthonous Tuscan series (referred to as the "tectonic wedges") and underlying core complex metamorphic formations (Carmignani and Kligfield, 1990; Block, 1991).

The Tectonic slices is part of the Monteciano-Roccastrada Unit (or Tuscan Metamorphic sequence). This Mesozoic-Paleozoic sequence is composed of three units, 1) quartz metaconglomerates, quartzites and phyllites, 2) phyllites and quartzites, and 3) micaschists. Underlying the Monteciano-Roccastrada formation lies a pre-Alpine gneiss complex interbedded with amphibolites (Ordovician-Silurian age). Metamorphism affecting this unit originated in the Hercynian Orogeny (approximately 300 m.a.) and included the formation of NE-SW trending fractures (Batini *et al.*, 1985a; Cameli *et al.*, 1993; Carmignani and Kligfield, 1990). The Gneiss and Monteciano-Roccastrada units are often referred to in the literature as being representative of the lower plate and the term "basement" has been applied to both.

The compressional stress that lead to the displacement of the Ligurid and Tuscan sedimentary sequences onto the core complex was followed by a period of post collisional extension (referred to by Carmignani and Kligfield as the D2 deformation). The late Tortonian (Miocene) D2 tensional stresses created boudinage structures within the cherty limestones of the metamorphic complex, attesting to the extensional affects at mid-crustal depths (below 3 km). Effects of the D2 deformation on the upper crust can be seen in the northwest-

erly trending extensional normal faults. Vertical displacement along these fractures created Horst-Graben structures into which sediments deposited during the Miocene and Pliocene (Neogene sediments) (Cameli et al., 1993; Carmignani and Kligfield, 1990).

The third episode of tectonic disturbance includes Pliocene and later age magmatism and volcanics. The D2 extensional deformation creating the NW-SE fractures migrated eastward across the Italian peninsula during the Pliocene and Quaternary times. The existence of the faulting provided flow pathways for later magmatism (Puxeddu, 1984). This magmatism is thought to be responsible for the formation of the Quaternary volcanics located in Tuscany as well as numerous granitic intrusions emplaced throughout the geothermal regions. It has been suggested that most of Tuscany is underlain by granitic type intrusions. Petrologic data suggest the age of origin of the accessible formations to be 2.5-3.5 ma. (Batini et al., 1985a).

The velocity model used in the relocation was developed using information from several sources. P and S wave velocities, and their ratios (Vp, Vs, and Vp/Vs) were based on results of a seismic reflection survey conducted by Batini, Duprat and Nicolich (1985), and on joint hypocenter-velocity inversion from local earthquake data conducted by Block (1991). The thicknesses for the layers were based on the seismic reflection results and on detailed contour maps of the primary units (Batini et al., 1985a,b; ENEL-Unita Nazionale Geotermica, 1988a,c,b; Societa Elaborazione Cartographiche, 1978a,b,c,d).

Batini, Duprat and Nicolich (1985) identified several seismically reflective horizons which correlate well with the Liguride, Tuscan, and "Basement" units. These horizons, identified as the "L", "T" and "B", respectively, were associated with velocities ranging from 4,000 m/s to 6,100+ m/s, with Vp/Vs ratios ranging from 1.7 to 1.9, depending upon the formation (Block, 1991; Batini et al., 1985b). In addition, another reflector, known as the "K" horizon, has been identified. It is regionally extensive, covering large areas in southern Tuscany and varies in depth from as shallow as 2.8 km in the southern Larderello geothermal field to greater than 9 km near Montalcinello (20 km east) and other locations (Cameli et al., 1993; ENEL-Unita Nazionale Geotermica, 1988a).

The "K" horizon is located within the gneissic basement, and although several possible interpretations regarding its nature have been proposed, its exact origin has not been clearly established. One interpretation suggests that the "K" horizon represents a zone of fracturation and the presence of fluid filled fractures (Batini et al., 1985b), while others have suggested that it represents a rheological boundary between the brittle upper unit and a ductile lower unit (Cameli et al., 1993). The seismic reflection results delineate sub-vertical normal faults which cross- cut all basement units including the gneissic formation and the "K" horizon (Batini et al., 1985a). Additionally, other sources indicate that normal listric faults flatten into the "K" horizon and conclude that the brittle-ductile boundary is kinematically active (Cameli et al., 1993).

In the southern portion of the Larderello geothermal field, the K horizon splits into several individual reflectors which are relatively shallow. A well, designated San Pompeo 2, penetrated through the Monteciano-Roccastrada Unit and the gneiss unit, into the upper portions of the "K" horizon. The basement units were found to be highly fractured to a depth of 2,300 m, where an impermeable phyllite and micaschist unit was encountered. At 2,930 m drilling progress stopped when the drill string encountered a zone of highly fractured rock with hydrothermal and contact metamorphism mineral assemblages, fluid pressures in excess of 240 bars (24 MPa) and temperatures in excess of 400C (Cappetti et al., 1985).

The Larderello Geothermal Field

The Larderello geothermal field is a vapor dominated, hydrothermal type field producing steam primarily from zones associated with the Triassic anhydrites at the base of the Tuscan nappe (Puxeddu et al., 1977). The geothermal source at Larderello is thought to be a granitic type intrusion at depths ranging from 6 km to greater than 25 km (Batini et al., 1985a; Block, 1991). In support of this theory is the identification of aplitic veinlets in samples from deep wells (Minissale, 1991) and a broad seismic velocity low extending from depths of approximately 7 km to 25 km, approximately the depth of the Moho (Block, 1991;

November 20, 1997 19:01

Carmignani and Kligfield, 1990).

Cameli *et al.* (1993) report that the occurence of seismicity within the boundaries of the Larderello geothermal area is concentrated between 1 and 7 km in depth, with a peak occurance between 3 and 5 km. This depth range correlates well with the "K" horizon, and with estimates from the relocations presented here. However, any interpretation of the cause of the events must account, not only for the horizontal and vertical placement, but also for the focal mechanism parameters. We offer an evaluation of each of these elements in the following discussion.

Only two previously identified geological structures are discussed in the literature for this area and depth range; the "K" horizon and the NW-SE trending, high angle, normal faults. A detailed map of the northern boundary of the Larderello field indicates that the "K" horizon is located between 4.4 and 5 km in depth and that the area is cross-cut by two of the normal faults (ENEL-Unita Nazionale Geotermica, 1988a). The horizontal location of the March 1993 cluster in relation to these features is shown in Figures 0-31 and 0-32.

A review of the focal mechanisms, spatial geometry and temporal distributions suggest that the microearthquakes in this cluster differ in overall character from those studied recently in regions of active volcanism, such as the Mid-Atlantic Ridge (MAR) and at convergent plate boundary volcanoes. In recent literature, the study of naturally occurring microearthquakes has been limited, in general, to events with magnitudes greater than 3.0 due to limitations imposed by the detection limits of the seismic networks. However, in these regions the events studied have been attributed to several specific mechanisms, including, dike emplacement, crustal extension, crustal loading, cooling and crystallization of magma, and magma withdrawal.

In the case of dike emplacement, the earthquakes have been observed to track the advancing magma front. Relocation of the Larderello earthquakes indicates no such temporal progressions and based on this, and on the lack of evidence supporting recent or active migration of magma at mid-crustal depths, we consider this mechanism as being an unlikely candidate

for these events.

In an evaluation of earthquake swarms on the MAR, Bergman and Soloman (1990) concluded that much of the seismicity detected exhibited normal faulting and is attributable to crustal extension, but that this conclusion is based primarily on events with magnitudes above the detection limit of the global seismic network (Mb=4.5). Dzurisin et al (1991) concluded that normal faulting and subsidence near the Medicine Lake Volcano, in Northern California is most likely due to crustal loading by the volcano and crustal thinning due to basin and range extension. In this study as well, the magnitudes of the events ranged between 3.0 and 4.6, and the focal mechanisms were different from those of the Larderello events.

The characteristics of the Larderello events are inconsistent with those observed at other volcanic areas, however, several other possible alternatives exist which take into account the unique nature of a cooling igneaous body. To evaluate these factors, we must clearly define the characteristics which must be accounted for. The focal mechanisms are the most consistent characteristic of the events and therefore we consider the two possible valid solutions identified earlier. The first is that the events occurred on one or more northwest striking faults which dip approximately 60 degrees to the northeast. Rakes ranging from 28 to 73 degrees indicate primarily reverse faulting with varying degrees of left lateral strike slip. The second alternative is that the events occur on south-southeast striking faults with varying degrees of dip to the west, and varying degrees of reverse and strike-slip components.

The horizontal location of the cluster and the first focal mechanism alternative strongly suggests an association between the events and the northern-most high angle fault, and taken along with the depth estimates, also indicates a possible interaction between the faults and the "K" horizon. The second alternative clearly excludes the northern-most high angle fault (due to an inconsistent dip direction), however, a potential association with the "K" horizon still exists.

Several pieces of evidence favor the first alternative. First, the correlation between strike

and dip of the fault plane solution and that of the existing faults in the gneissic unit is compelling, however, it remains to be explained how the D2 normal faults might be reactivated in reverse faulting. One possibility is that subsidence or downwarping of the "K" horizon is occurring due to cooling and or a drop in pore pressure due to steam migration. Another possibility is that microearthquakes represent only small displacements and therefore, the focal mechanisms for these events are most reasonably associated with very local phenomena rather than regional ones. The seeming inconsistency between the reverse faulting mechanism and the regional extension is therefore not a critical barrier to this alternative. In light of this, we might consider the events to represent displacement of small blocks within or near the fault zone with parallel or sub-parallel surfaces. Figures 0-24 through 0-27 seem to support a connection with the two fault directions apparent in the gneissic unit as observed by Carmignani and Kligfield (1990).

0.2.5 Discussion

The results of the relocation of the March 1993 Larderello microearthquake cluster place the events near the northern boundary of the vapor-dominated geothermal reservoir. Proximity of the cluster to a Tortonian age normal fault and the seismic reflector referred to as the "K" horizon suggest a complex interaction between the structures, temerature changes, and the hydrologic conditions at the geothermal field. I propose that these events may be associated with thermal contraction of the granitic body. I make this proposal based on the focal mechanisms indicating reverse faulting and the spatial association with pre-existing structures.

November 20, 1997 19:01

0.3 CONCLUSIONS

Our work on the 1993 microearthquake swarm at the Larderello geothermal field suggests that the most significant obstacle to the practical application of correlation techniques such as EGFs or relative event location for seismic events recorded at regional distances is due to the degree of waveform complexity that is related solely to scattering affects along the path. In this study we showed that dispite similar focal mechanisms and a regional scale that is on the order of 1 to 2 wavelengths, the complexity of the waveforms was severe, particularly for S waves. We showed that the event waveform types exhibited at least two distinctly different characters, thus forcing the use of more than one master event.

Our initial analysis of the cluster size suggested that for P waves the pertinent wavelengths were below 1220 meters, based upon a P wave velocity of 6100 m/s, with a mean wavelength of approximately 700 meters. The pertinent wavelength scale for S waves was below 700 meters so we expected to have more difficulty with the S wave correlation coefficients. Although the size of the overall cluster exceeded these bounds, the smaller subsets were of the required size (that being approximaltely one wavelength).

Another difficulty arose with the application of windowing around an absolute arrival time pick. This method was applied in an effort to bracket the true arrival time and to reduce the computing operations by limiting the lengths of the data sequences being correlated. The existence of strong scatterers introduced a significant difficulty in choosing the correct arrival and limited the window size, thus potentially affecting the accuracy of the correlation coefficient.

The difficulties discussed above were partially mitigated by a very careful and detailed analysis of correlation coefficients between master and slave events and multiple pass culling of the rms residuals from the inversion results. This effort clearly reduces the efficiency with which these techniques can be applied to large clusters and presents some new challenges in developing practical algorithms. However, in the case of the Larderello 1993 cluster, we are encouraged that the final result so clearly agreed with know geologic structures. This

suggests that refinements of the correlation techniques, in ways that reduce the effects of scattering, may further improve the results. One possible direction may be to introduce more thorough modeling of the scattered wavefield and removal of the non-essential phases from the waveform. This may improve the correlation coefficients by increasing the usable window length.

November 20, 1997 19:01

0.4 FIGURES
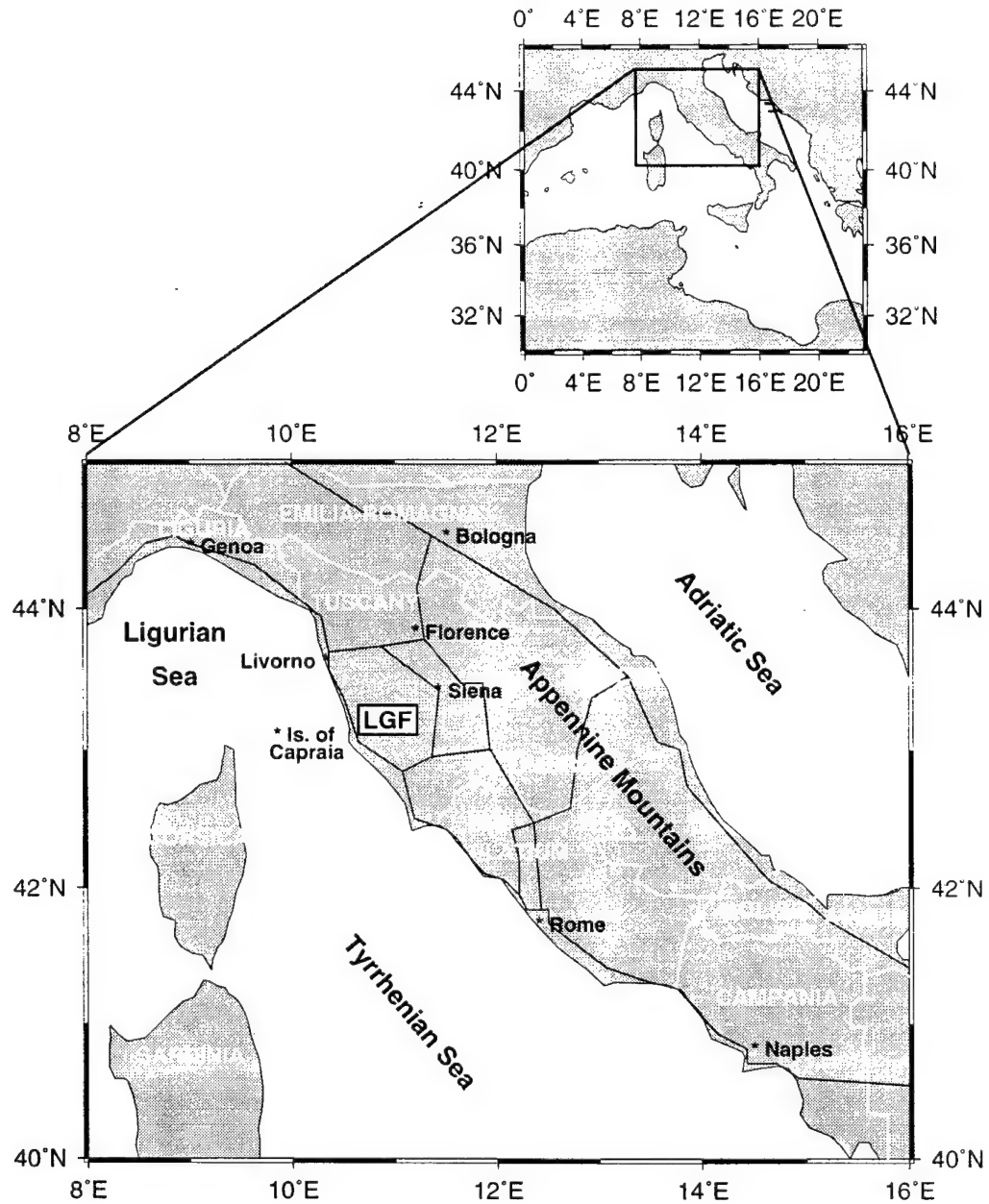
Figure 0-1: The Larderello Geothermal Field
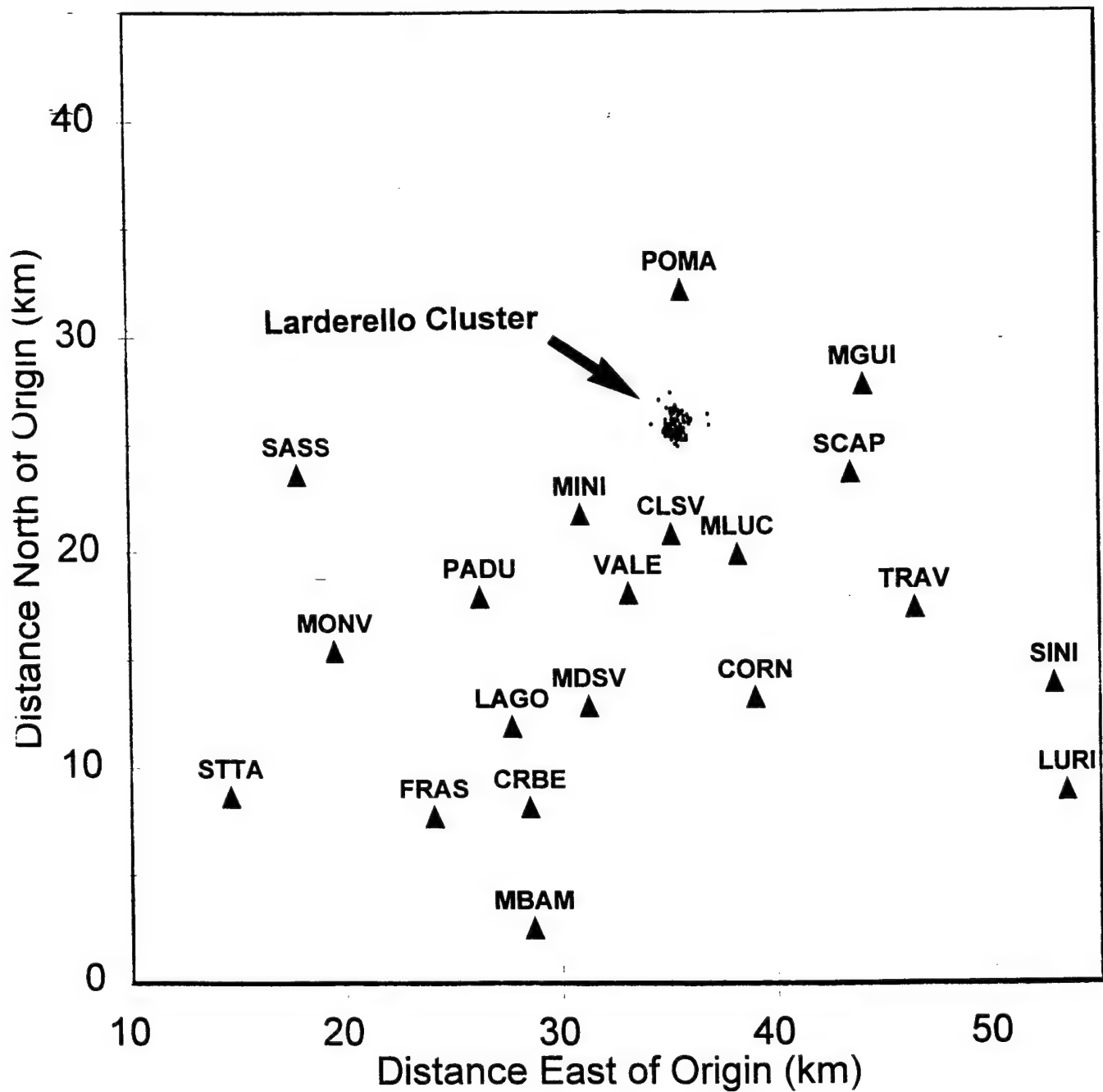
Figure 0-2: The Larderello seismic network (triangles) and the location of the cluster as determined by ENEL. The origin is located at Latitude 43N2'35", Longitude 10E29'58".
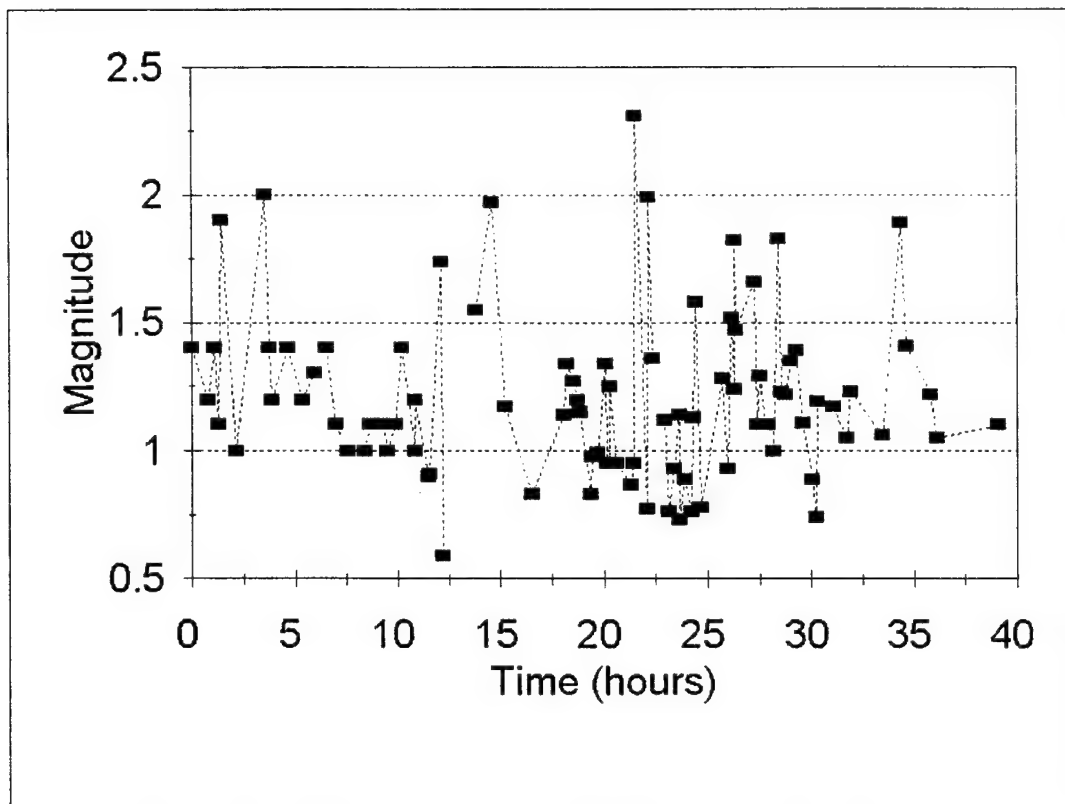
Figure 0-3: Magnitudes versus time for a subset of the March 20-23, 1993 Larderello microearthquake cluster.
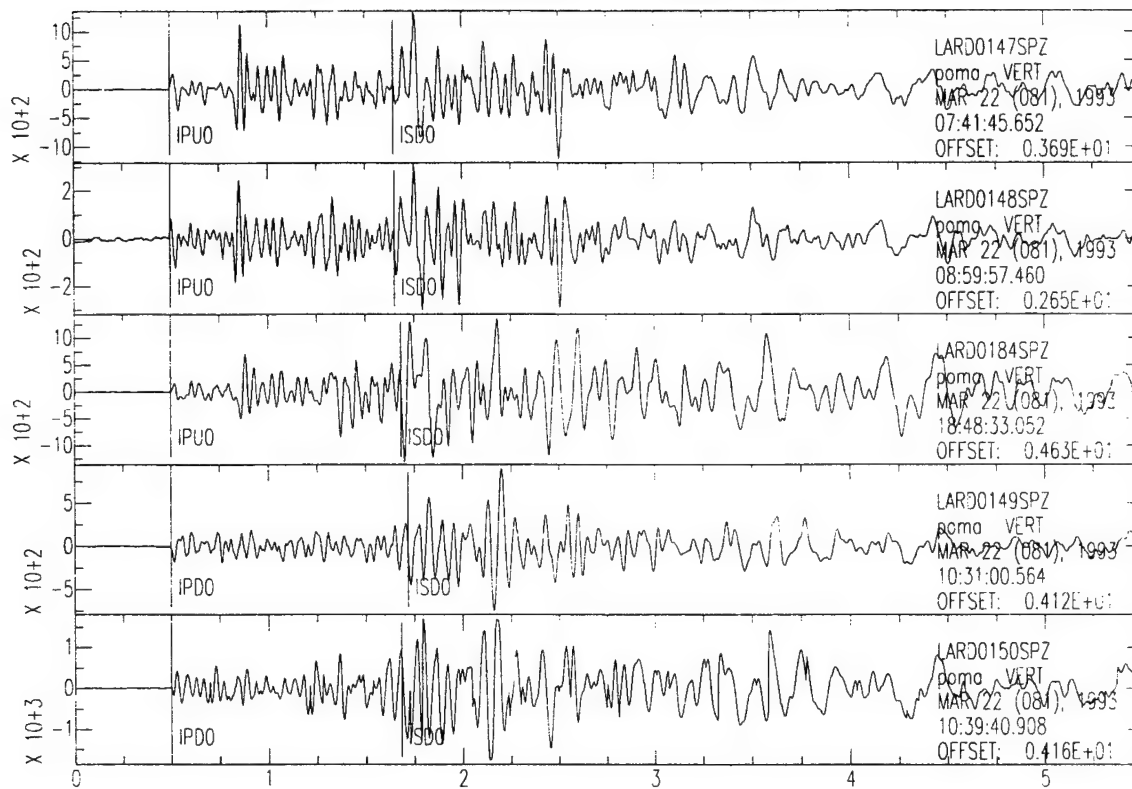
Figure 0-4: Five synchronized records from the station POMA showing P and S arrivals.
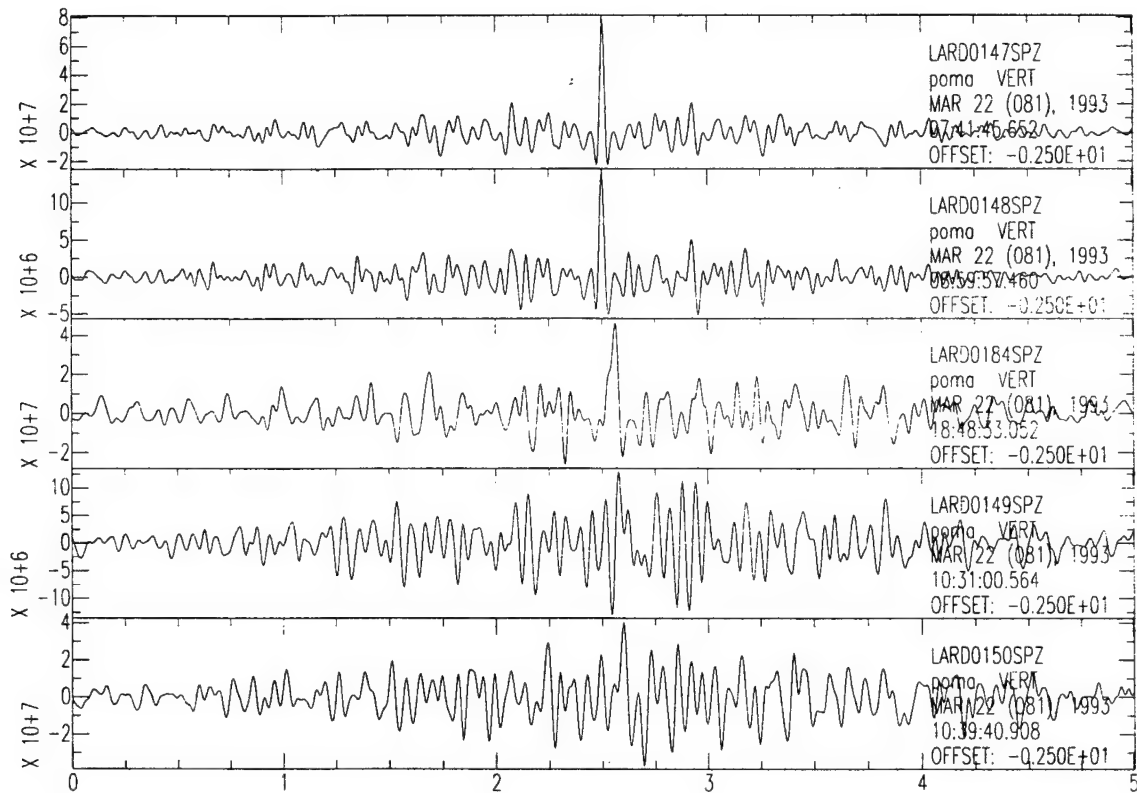
Figure 0-5: Cross-covariances of waveforms from five events with the waveform from event 147 (type II). Note that the record for 147 is therefore the auto-covariance function.
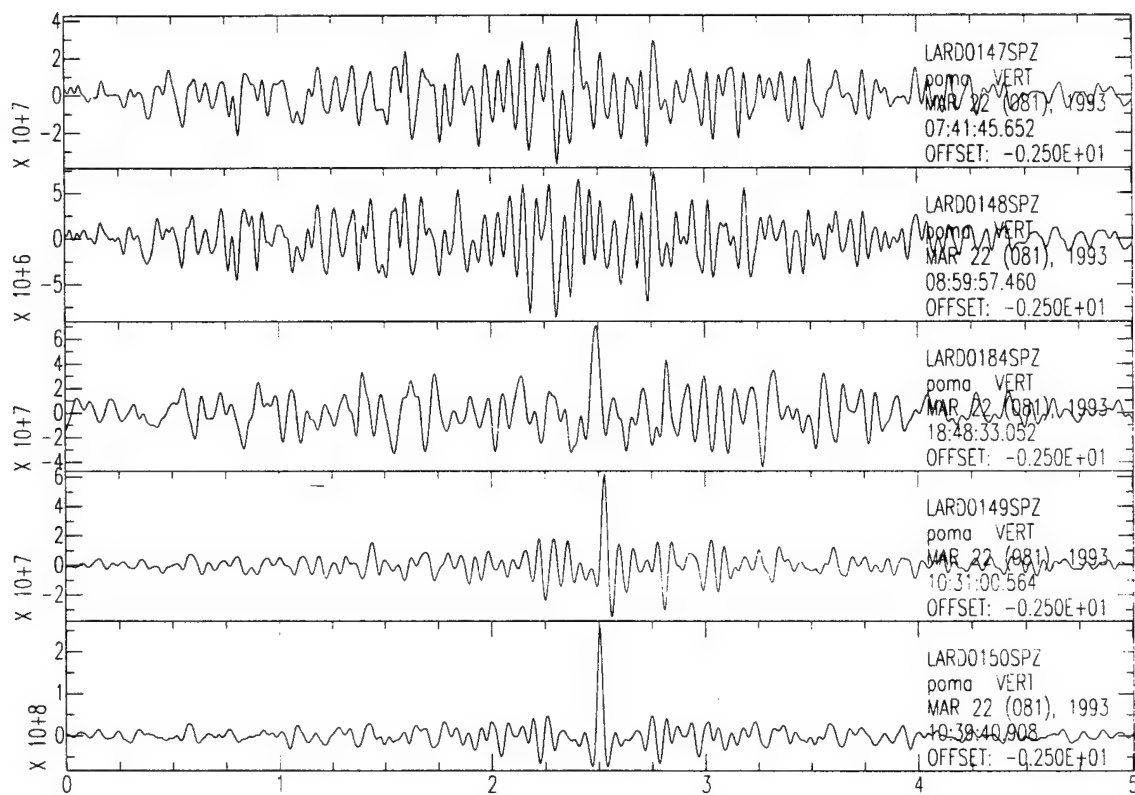
Figure 0-6: Cross-covariances of waveforms from five events with the waveform from event 150 (type I). Note that the record for 150 is therefore the auto-covariance function.
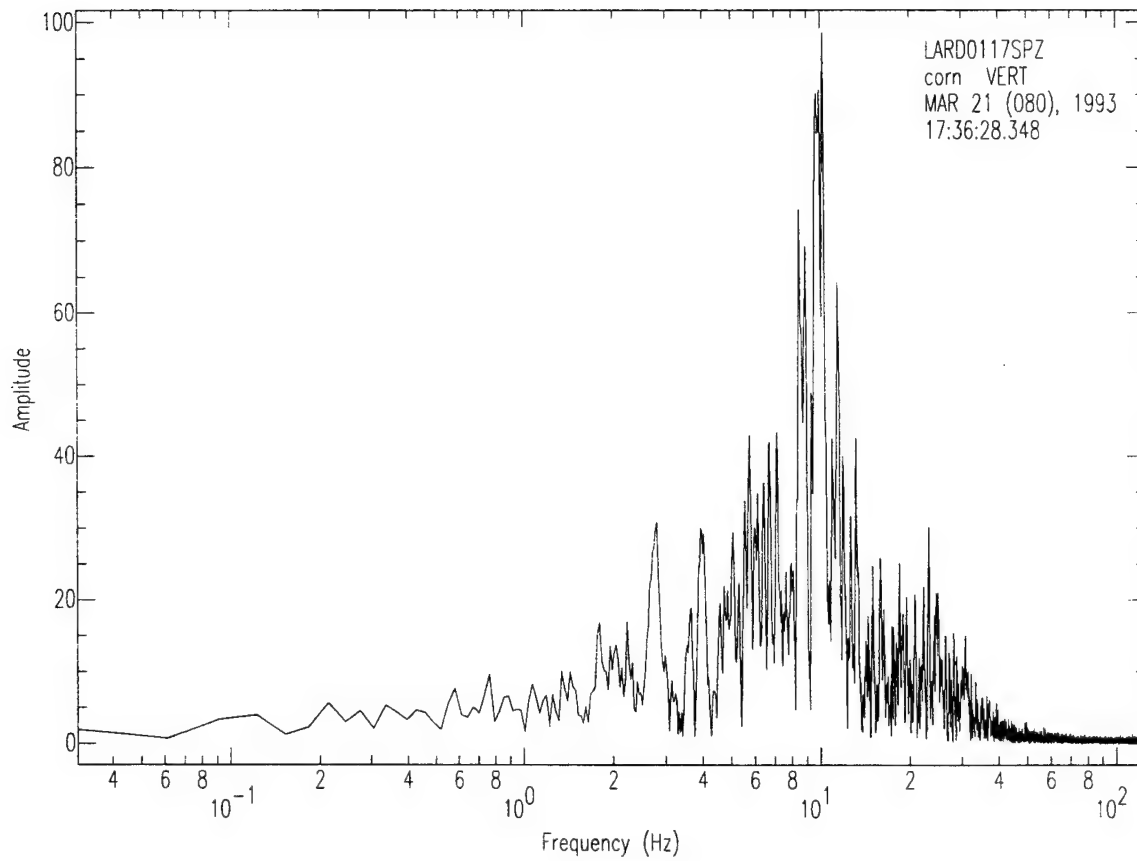
Figure 0-7: Amplitude spectra for event 117 at station CORN.
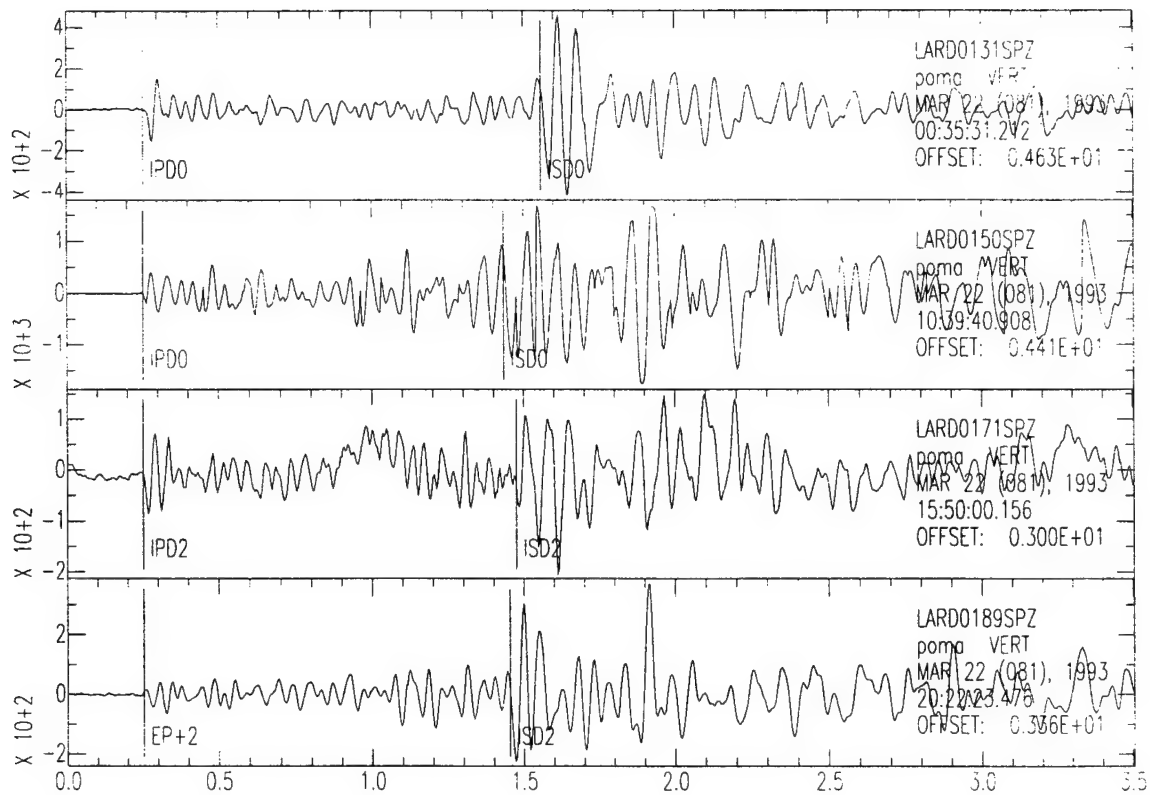
Figure 0-8: Master events of Type I for station POMA.
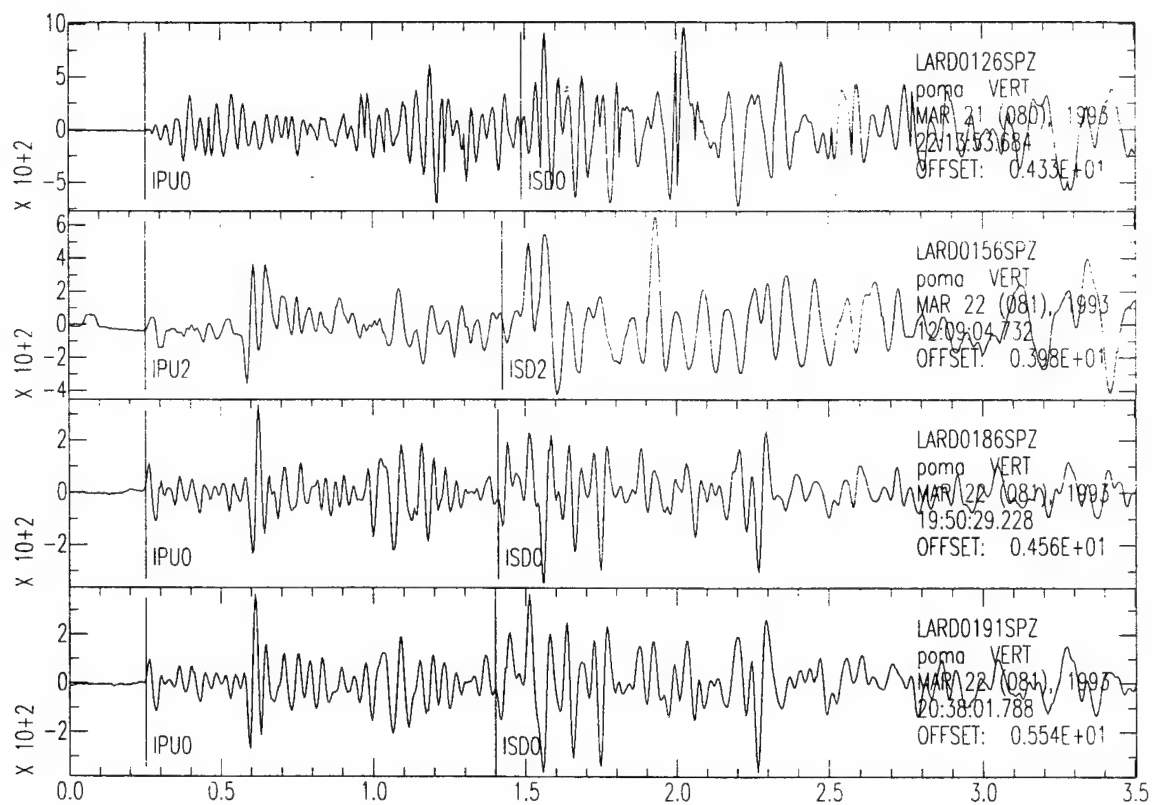
Figure 0-9: Master events of Type II for station POMA.
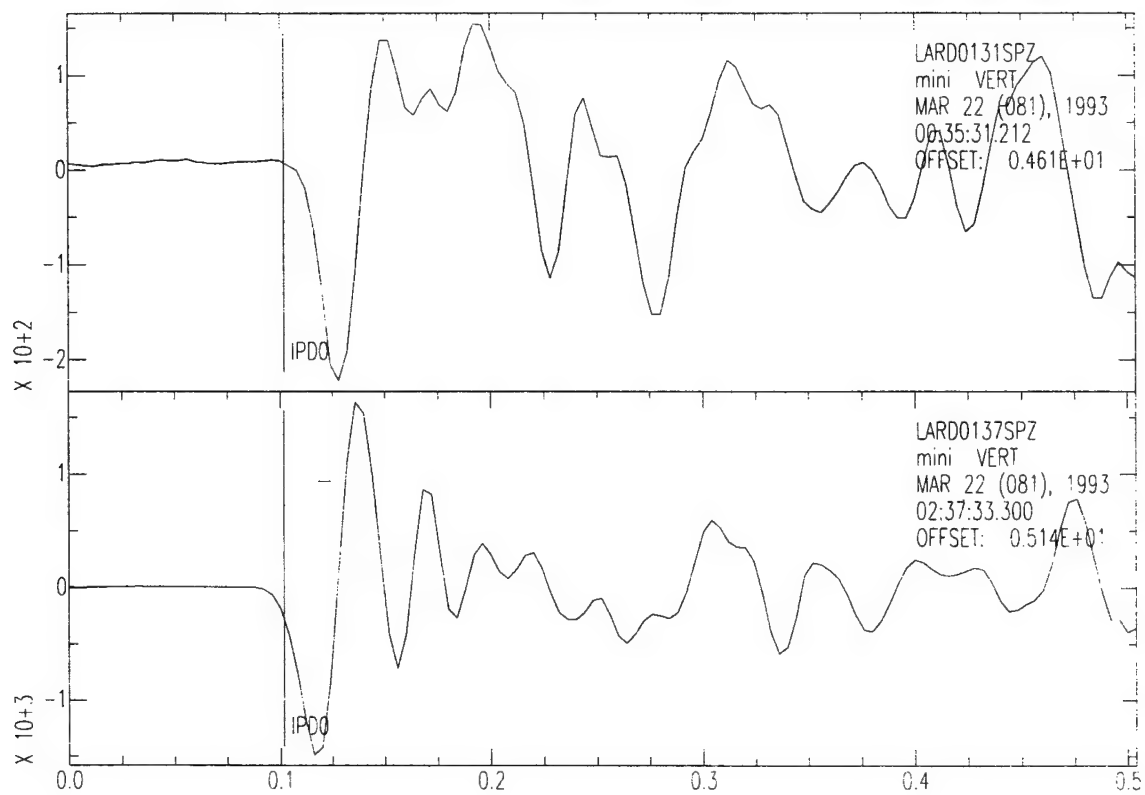
Figure 0-10: P wave windows for a master and slave event pair (unfiltered).
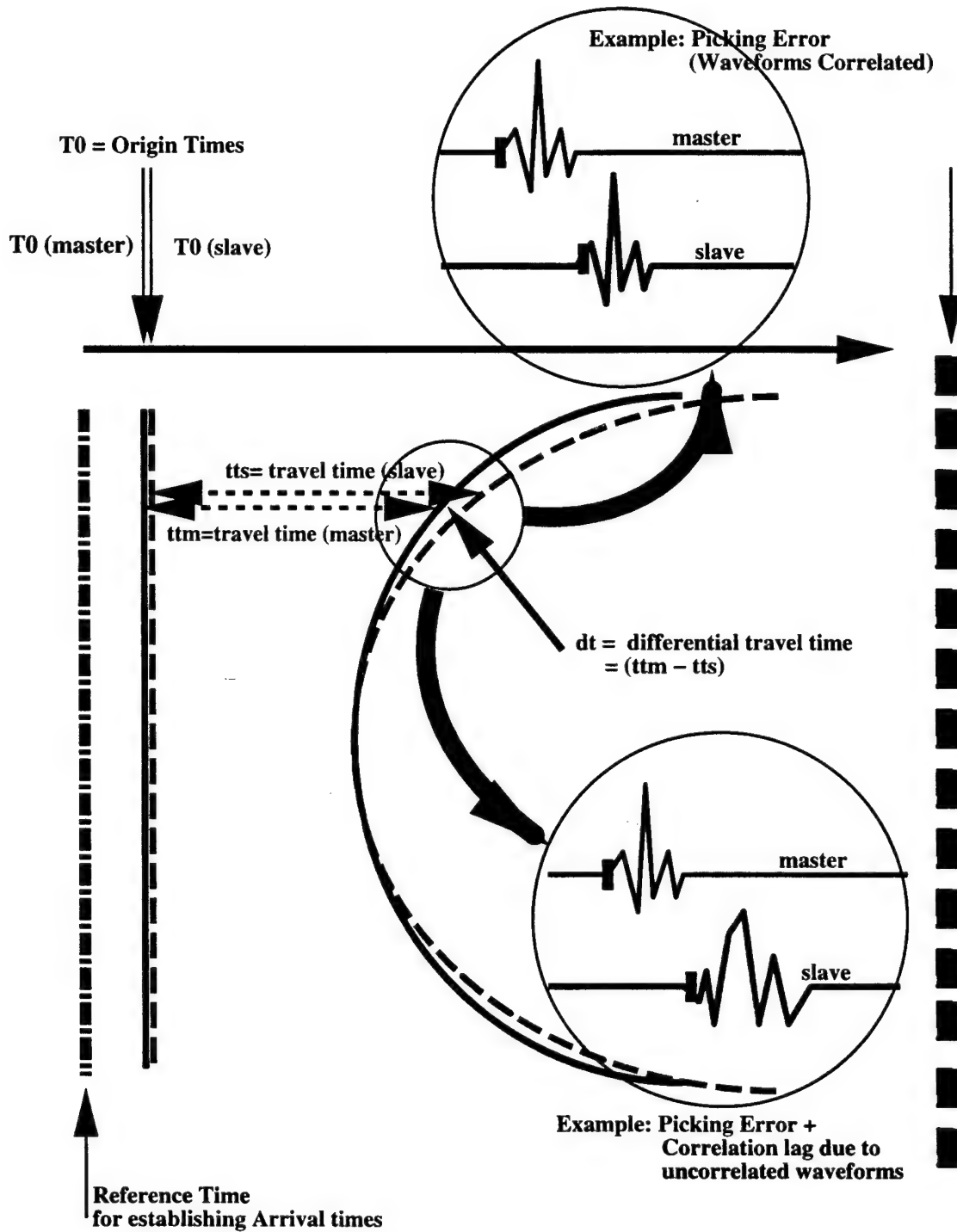
Figure 0-11: Schematic presentation of differential travel time elements.
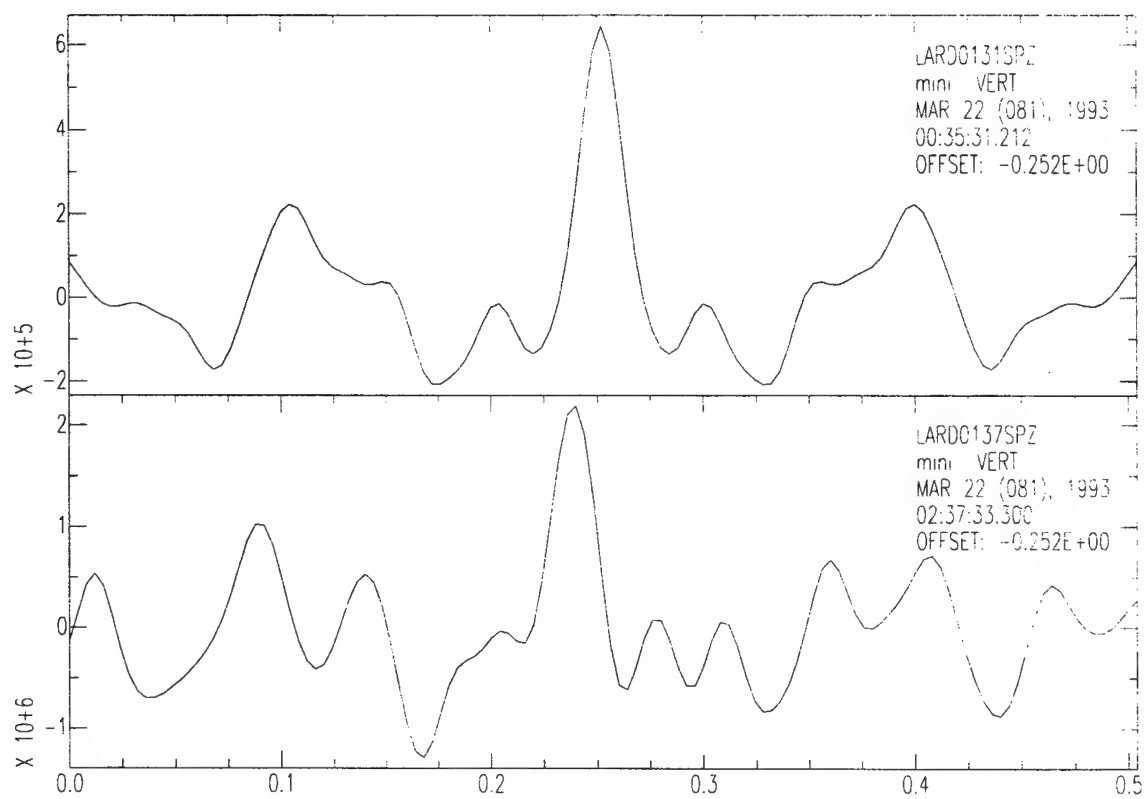
Figure 0-12: Auto- and cross-covariances of P wave windows for a master and slave pair (filtered and window-tapered).
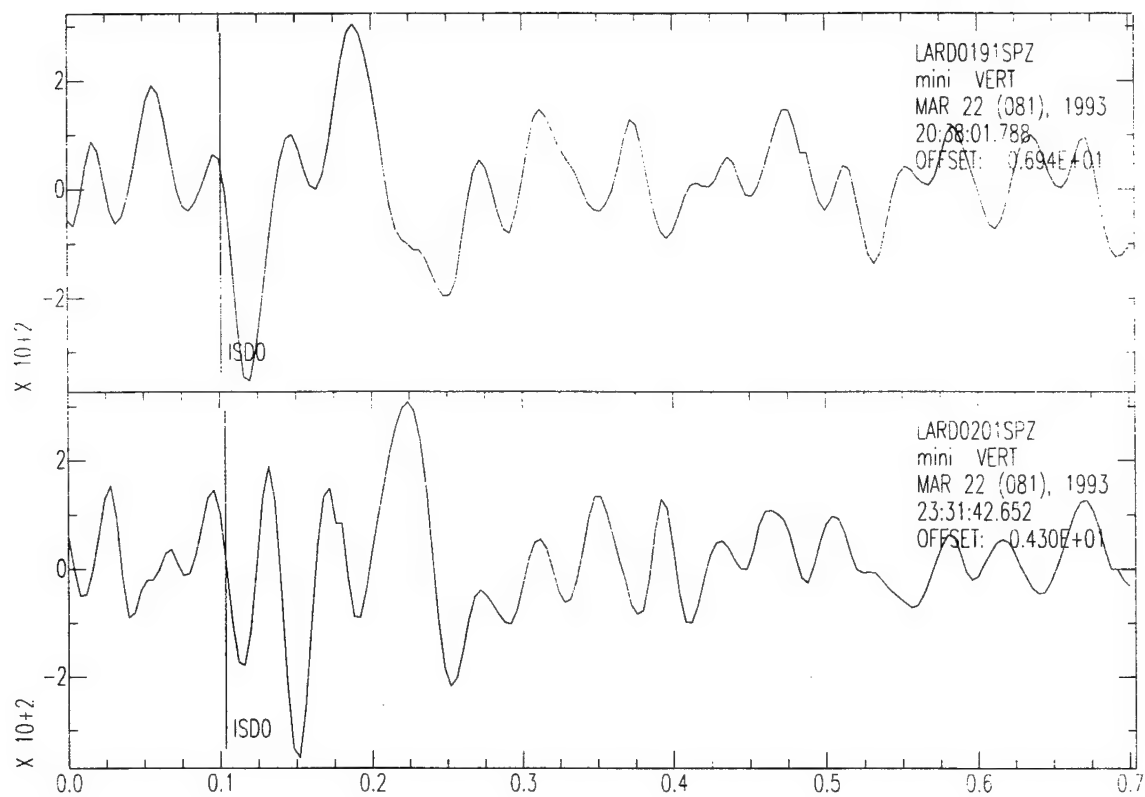
Figure 0-13: S wave windows for a master and slave event pair (unfiltered).
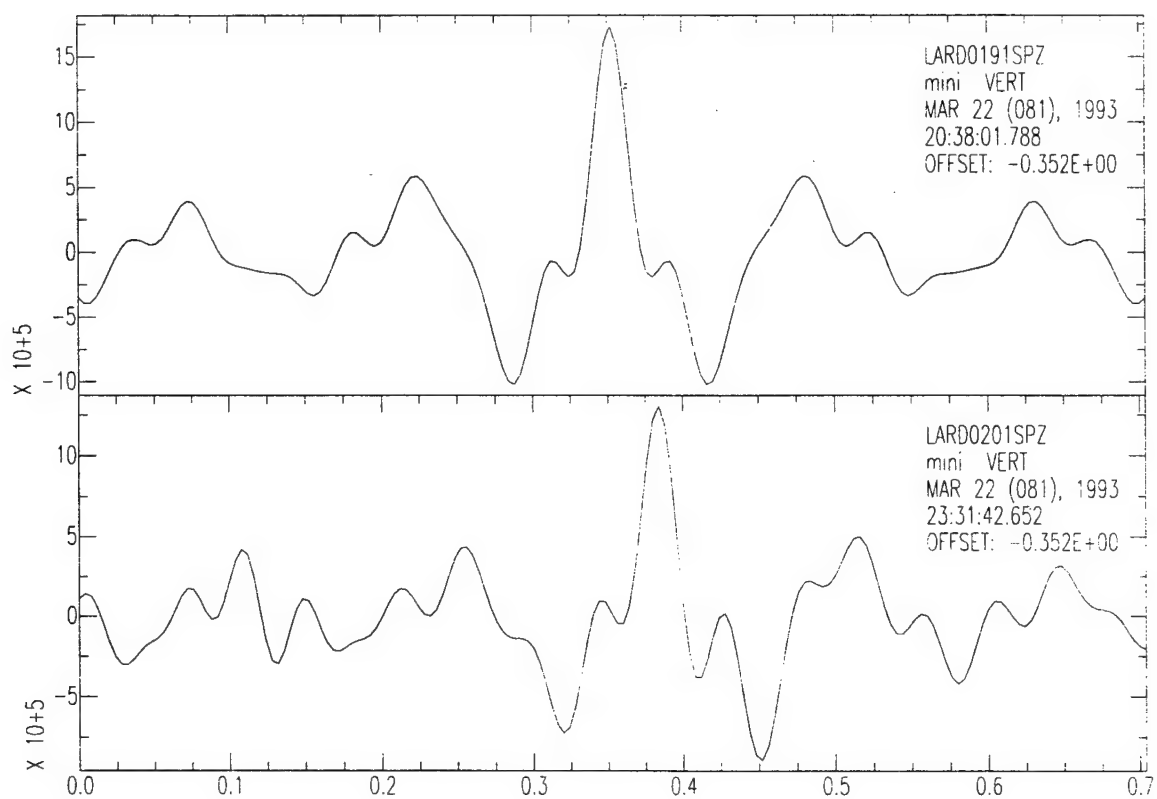
Figure 0-14: Auto- and cross-covariances of S wave windows for a master and slave pair (filtered and window-tapered).
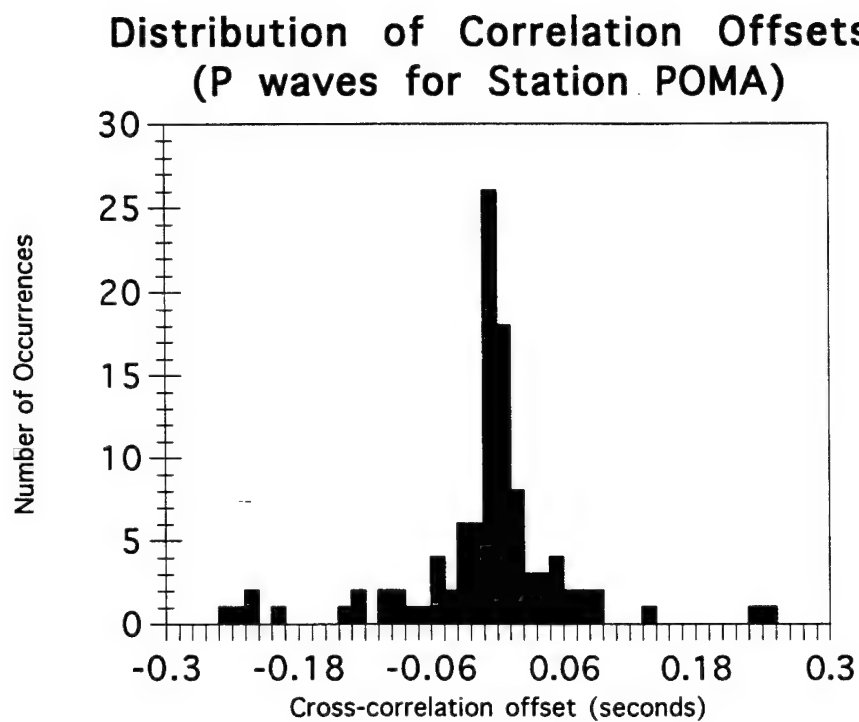
Figure 0-15: Distribution of cross-correlation offsets for P wave windows (86 events at station POMA).

Distribution of Correlation Offsets
(S waves for Station POMA)
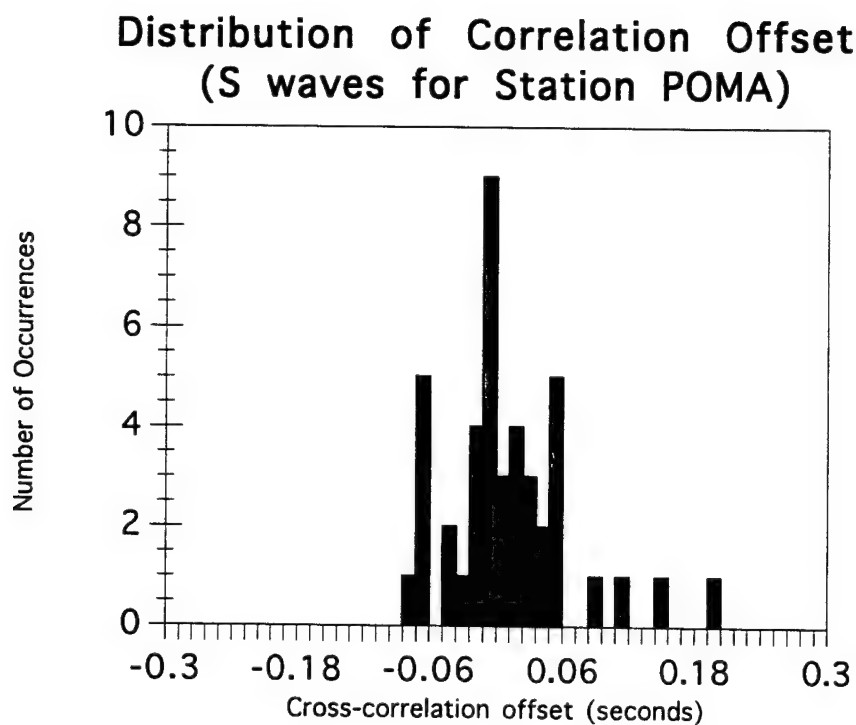
Figure 0-16: Distribution of cross-correlation offsets for S wave windows (86 events at station POMA).

Larderello Cluster Location
Estimates by relative picks (ttoff)
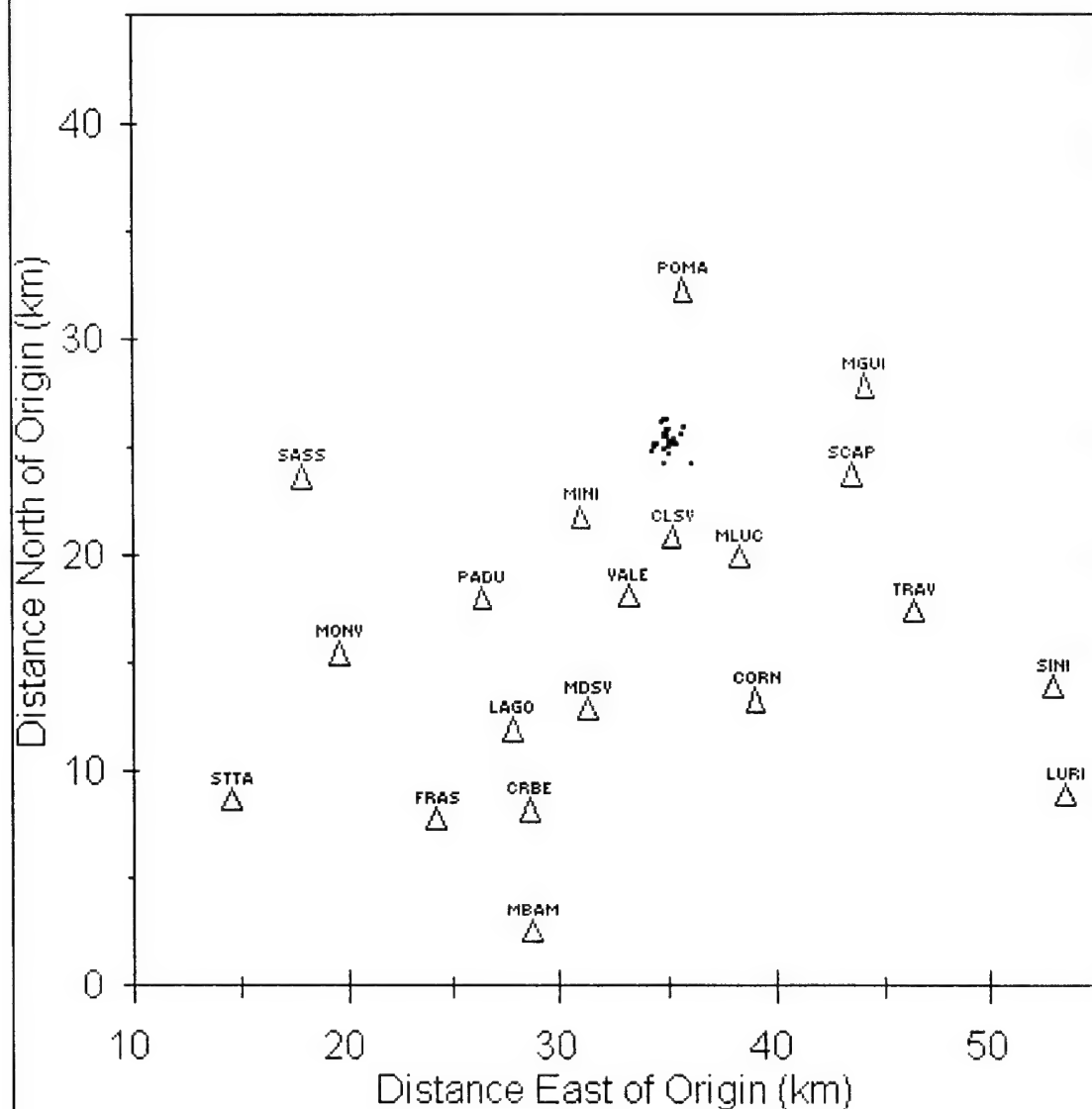
Figure 0-17: Map view of 86 relocated events from the March Larderello microearthquake cluster.

November 20, 1997 18:39

Larderello Cluster Location
Estimates by relative picks (ttoff)
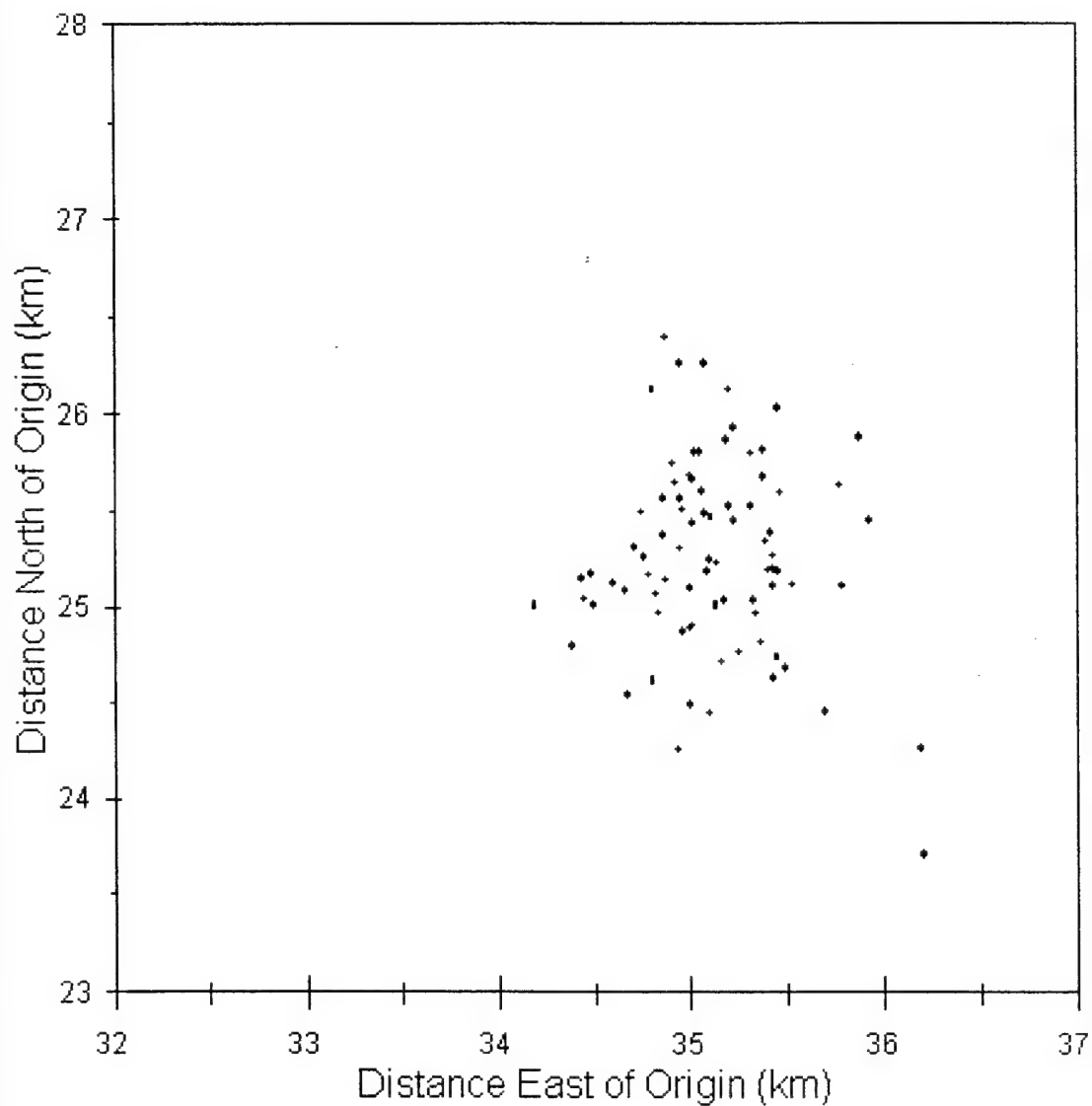
Figure 0-18: Local map view of the 86 relocated events.

Larderello Cluster Location
Estimates by relative picks (ttoff)
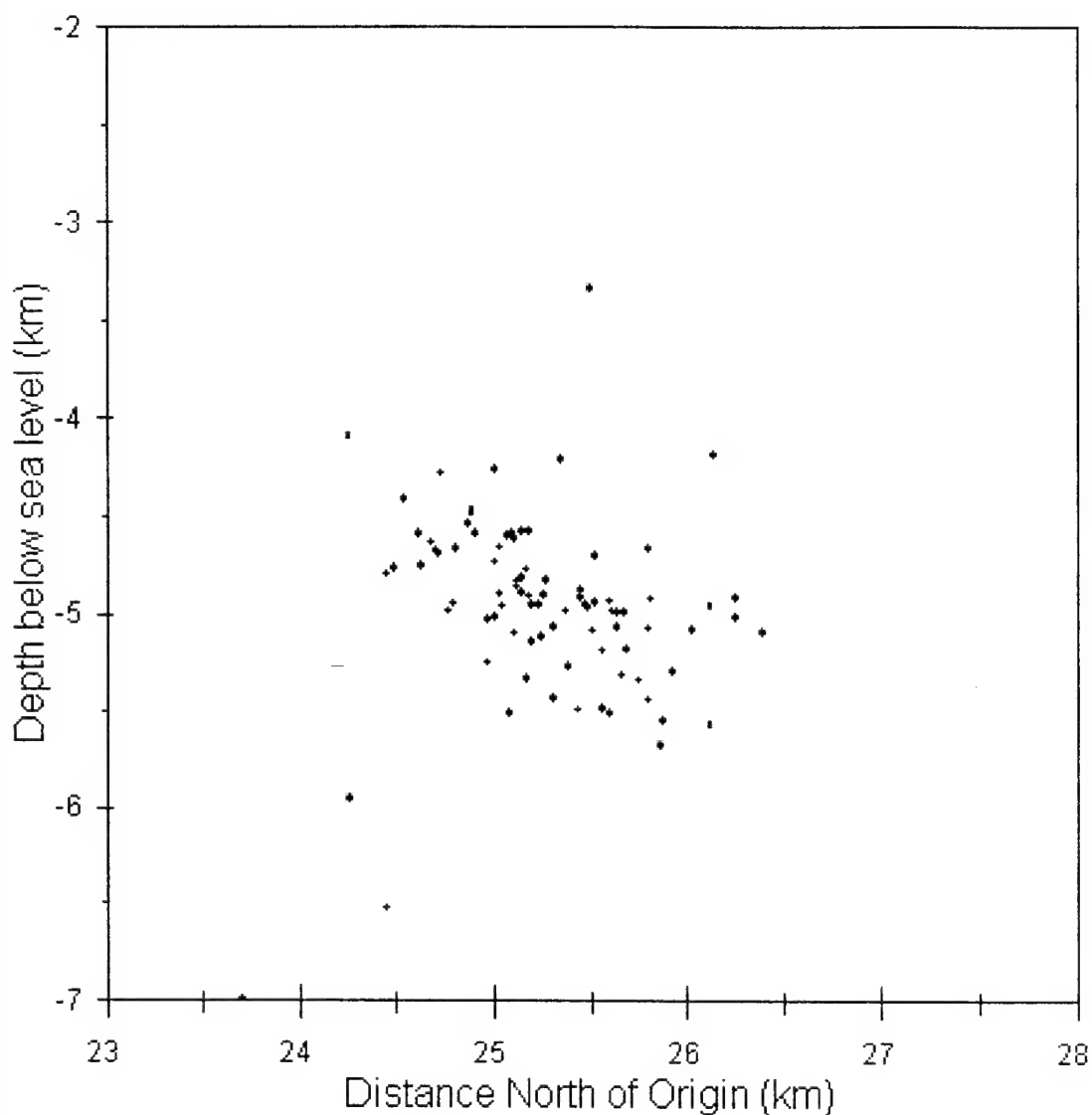
Figure 0-19: Cross-sectional view of the 86 relocated events, view looking west in depth section.
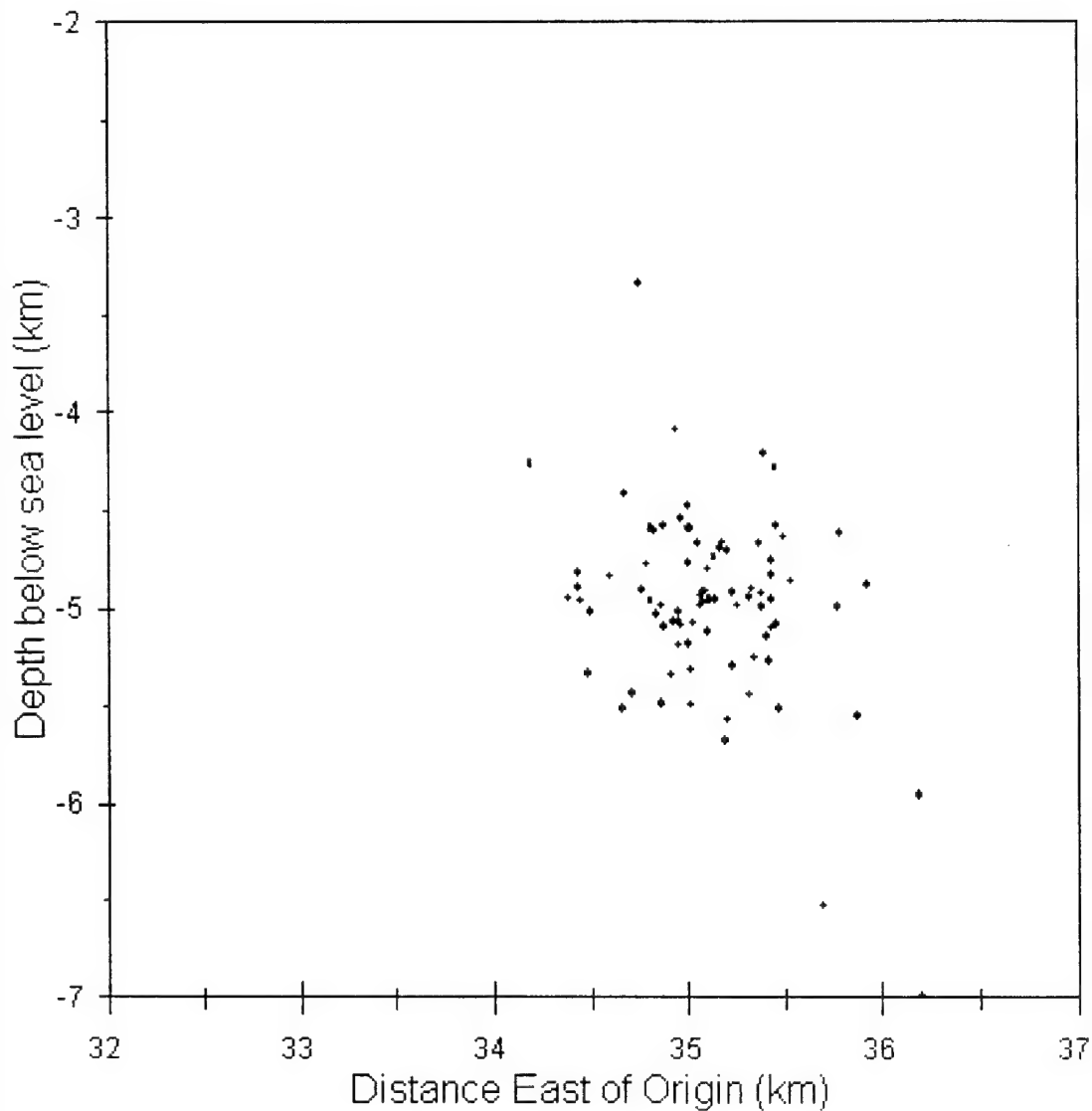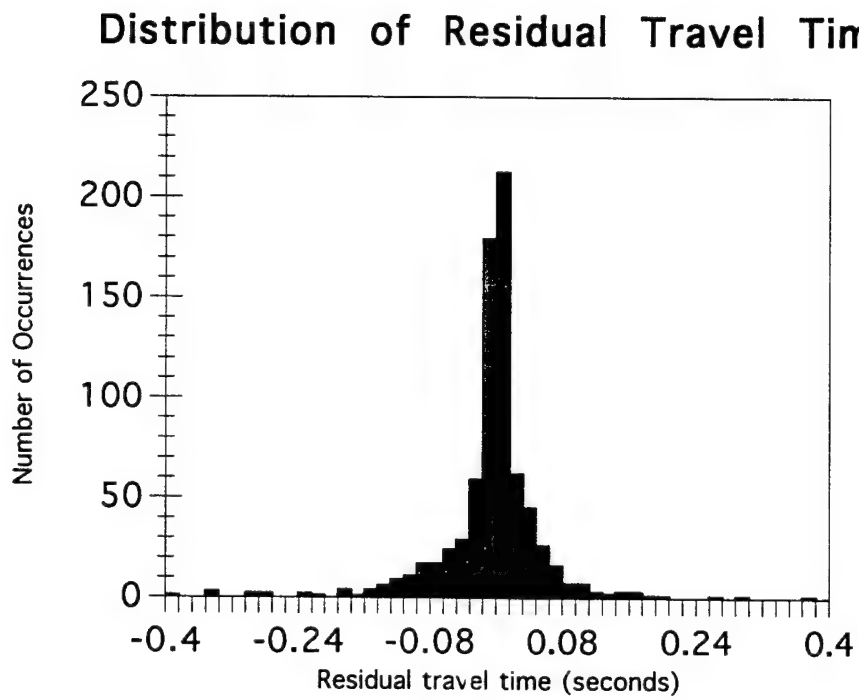
Figure 0-20: Cross-sectional view of the 86 relocated events, view looking north in depth section.

Distribution of Residual Travel Times

Figure 0-21: Distribution of traveltime residuals from the relative event location inversion of 86 events.

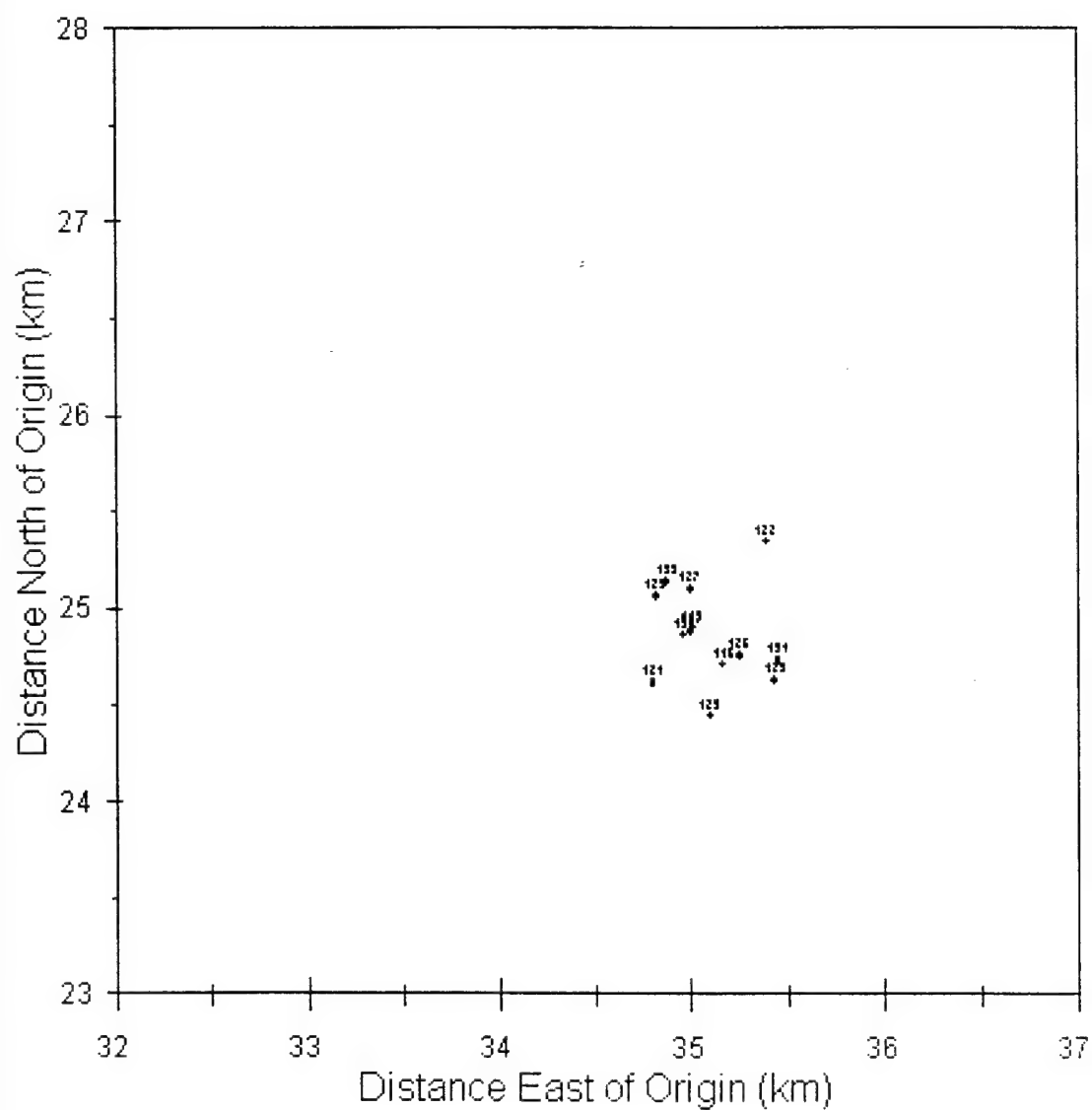# Larderello Cluster Location
Events 116-140 (culled relatives)

Figure 0-22: Map view of events in sub-set 1, events 116 through 140.

Larderello Cluster Location
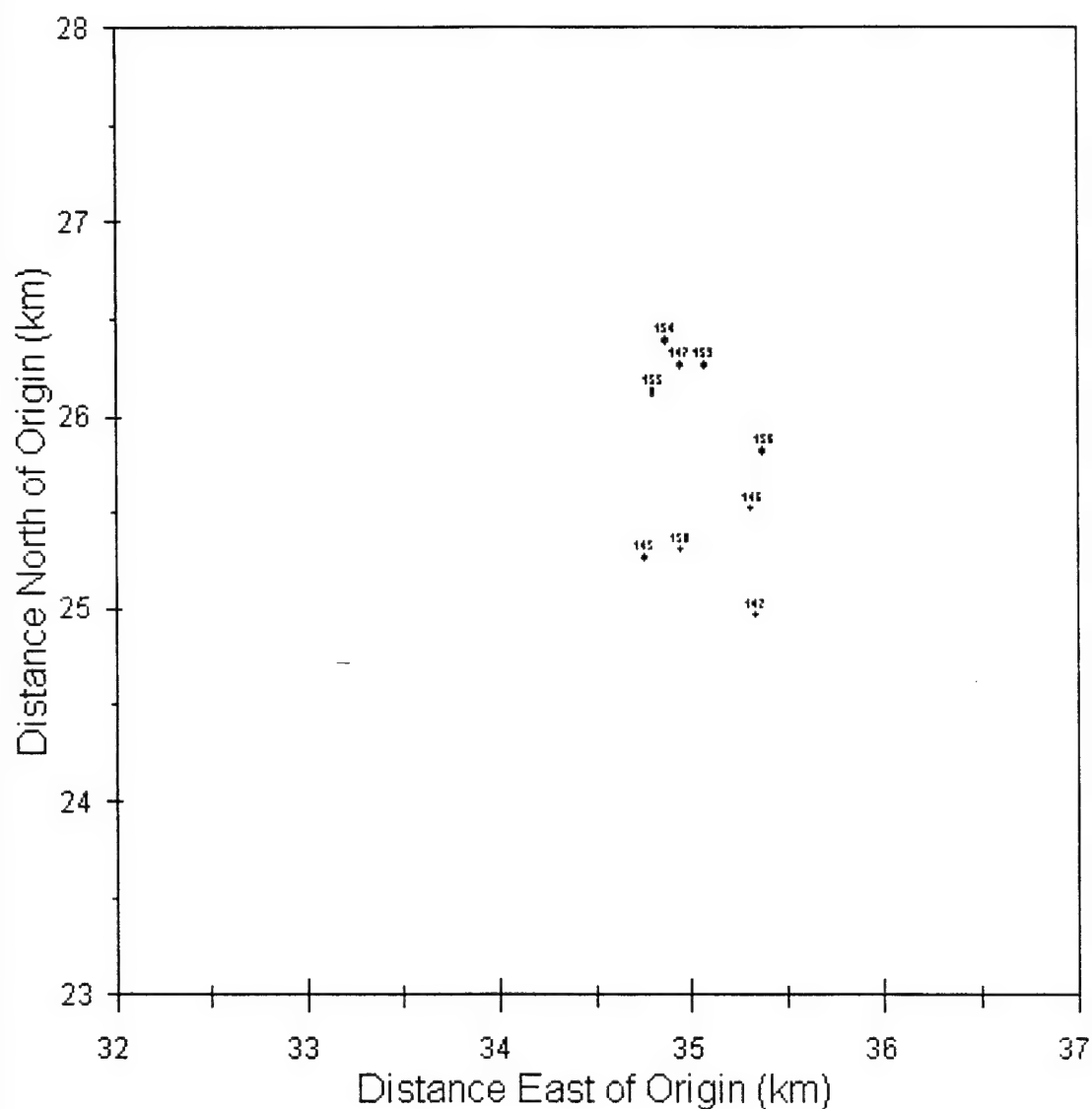## Events 141-156 (culled relatives)

Figure 0-23: Map view of events in sub-set 2, events 141 through 156.

Larderello Cluster Location
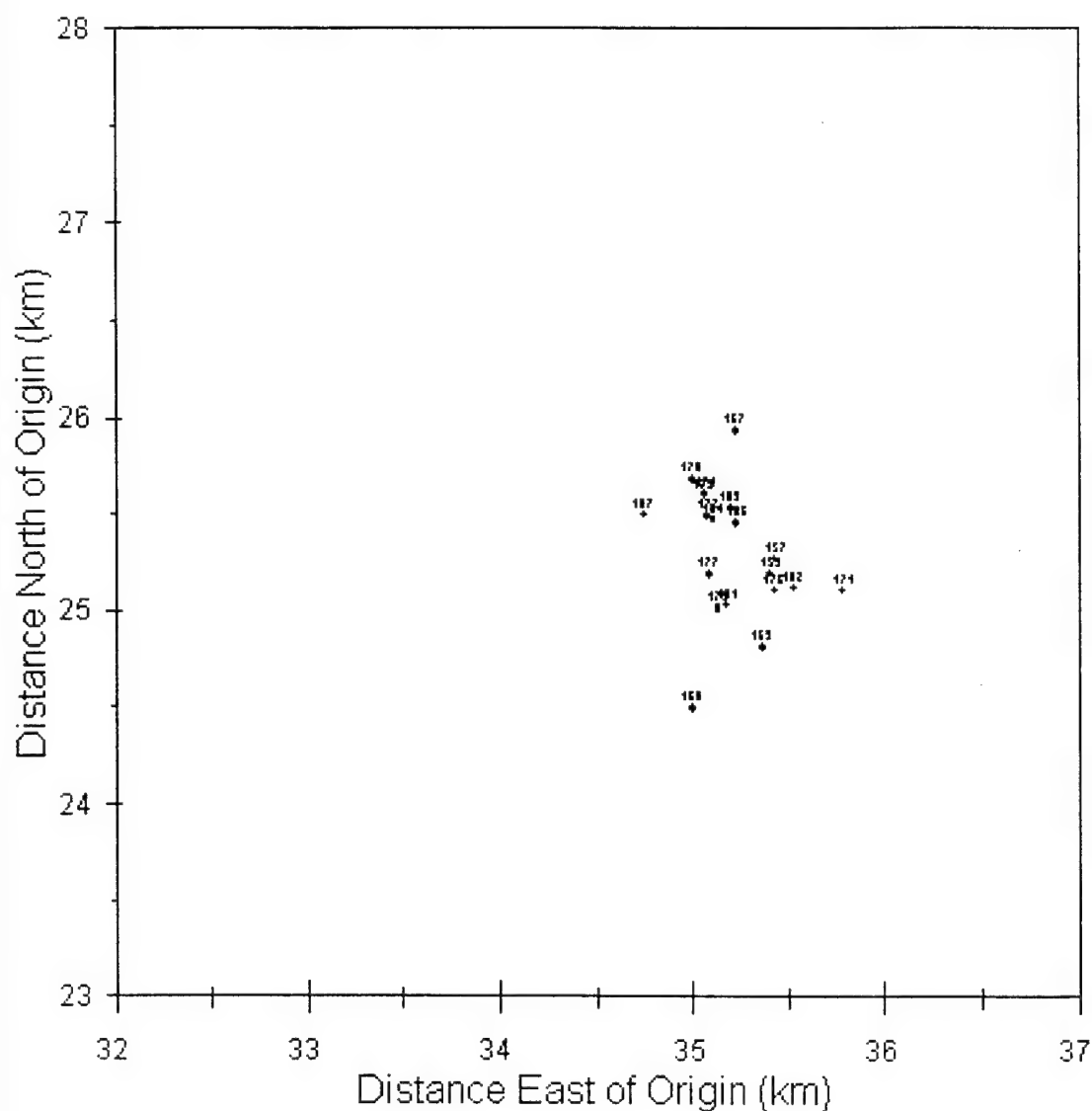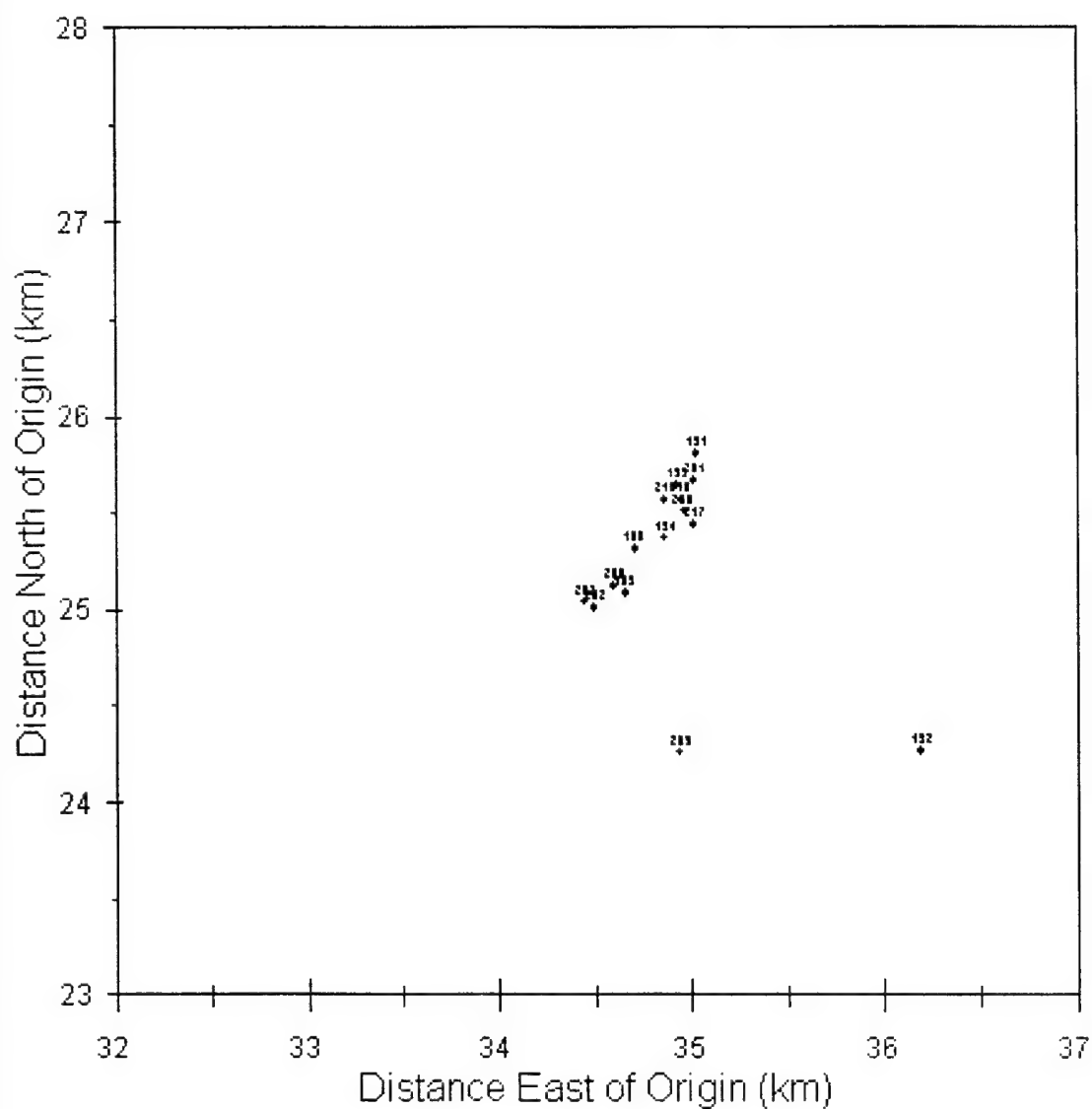## Events 157-187 (culled relatives)

Figure 0-24: Map view of events in sub-set 3, events 157 through 187.

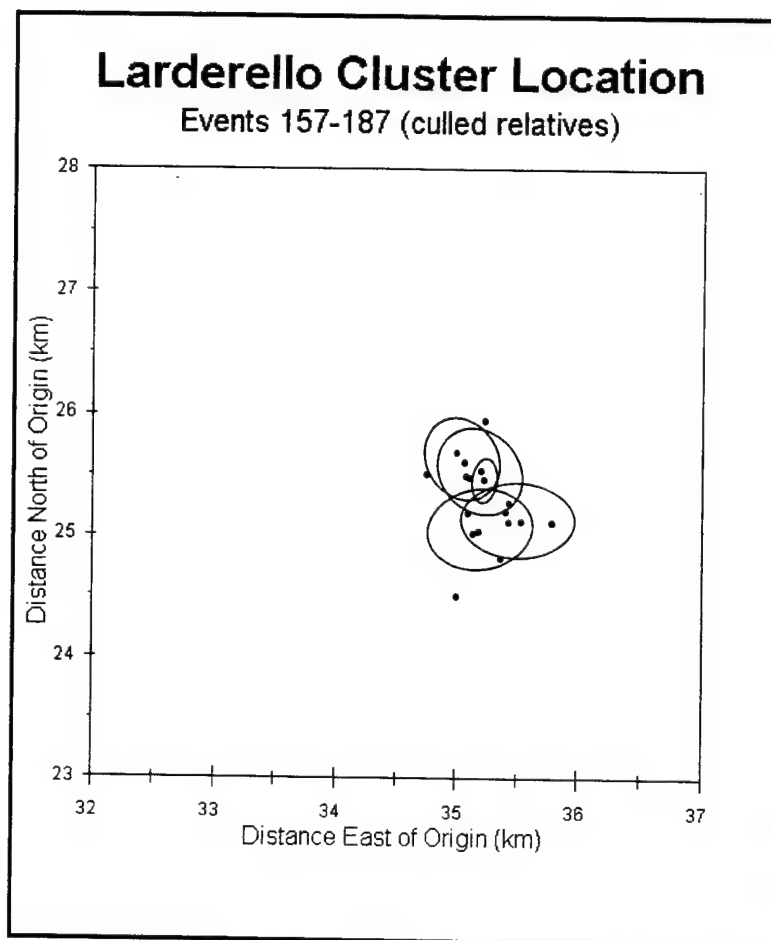# Larderello Cluster Location
Events 188-218 (culled relatives)

Figure 0-25: Map view of events in sub-set 4, events 188 through 218.

Larderello Cluster Location

Events 157-187 (culled relatives)

Figure 0-26: Estimated error ellipses for selected events from subset 157-187 showing typical values.

Larderello Cluster Location

Events 188-218 (culled relatives)

Figure 0-27: Estimated error ellipses for selected events from subset 188-218 showing typical values.
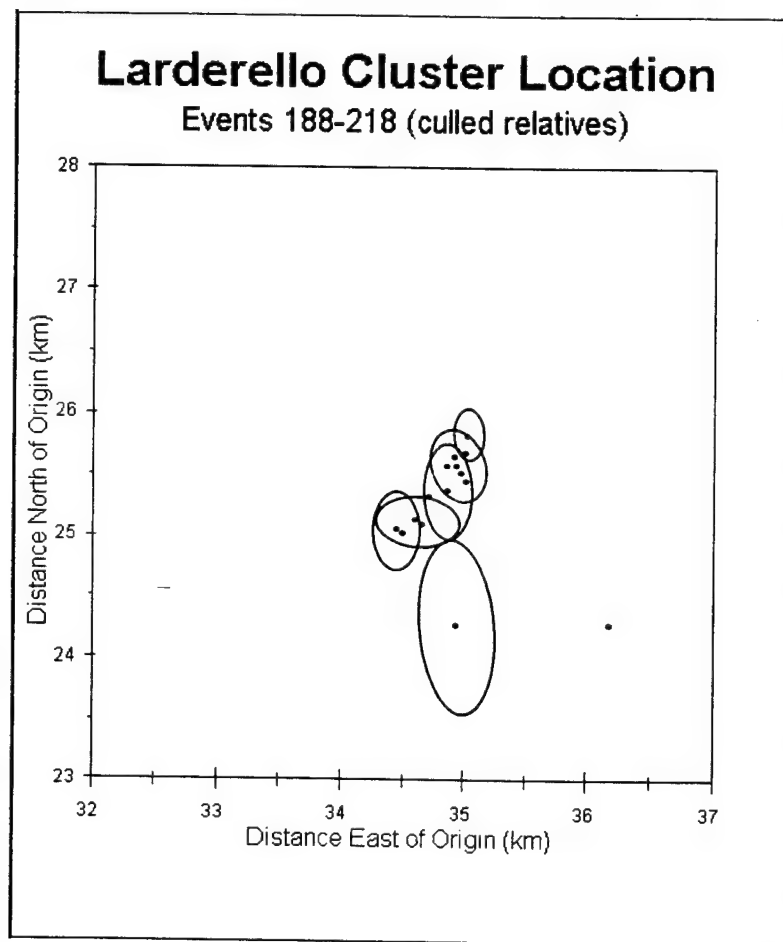
Larderello Cluster Location

Events 157-187 (culled relatives)
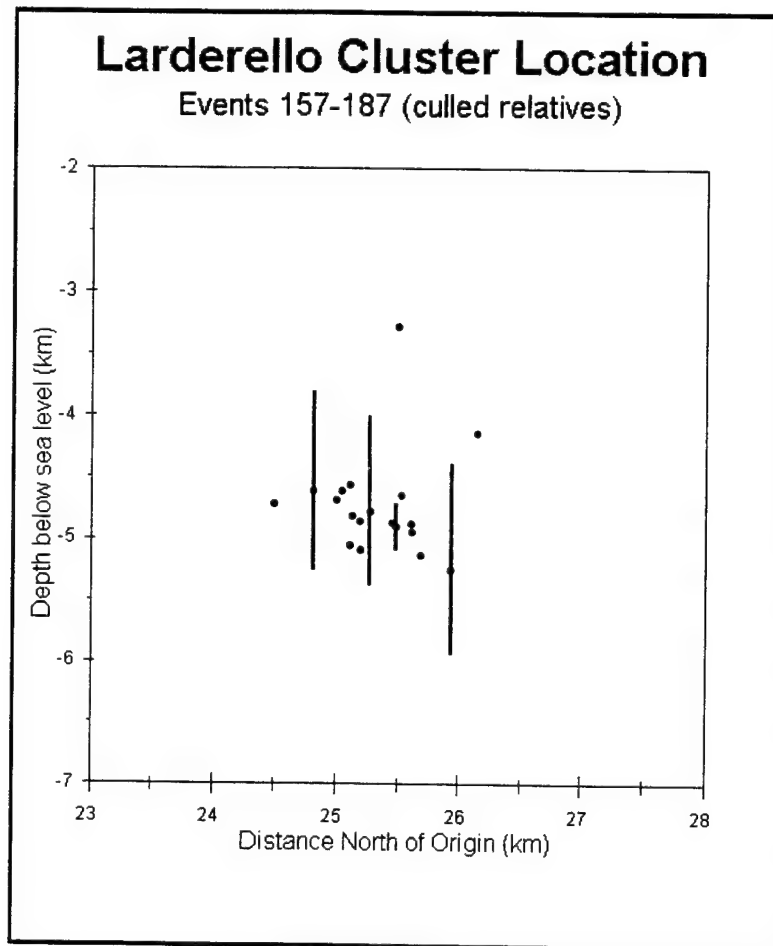
Figure 0-28: Estimated error bars for selected events from subset 157-187 showing typical values.

Larderello Cluster Location

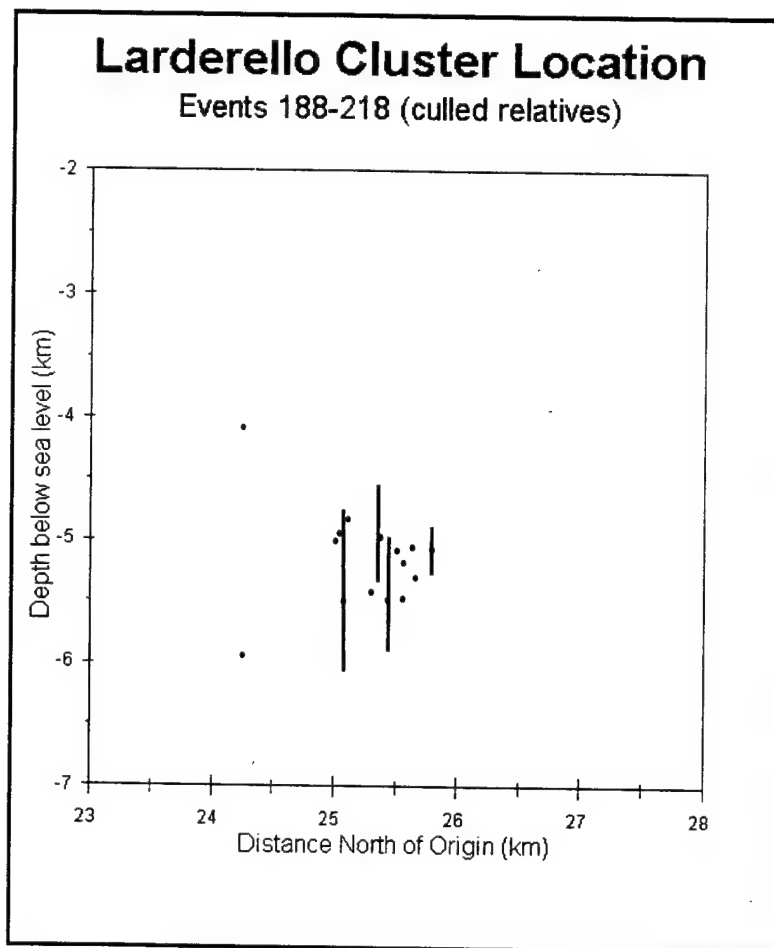Events 188-218 (culled relatives)

Figure 0-29: Estimated error bars for selected events from subset 188-218 showing typical values.
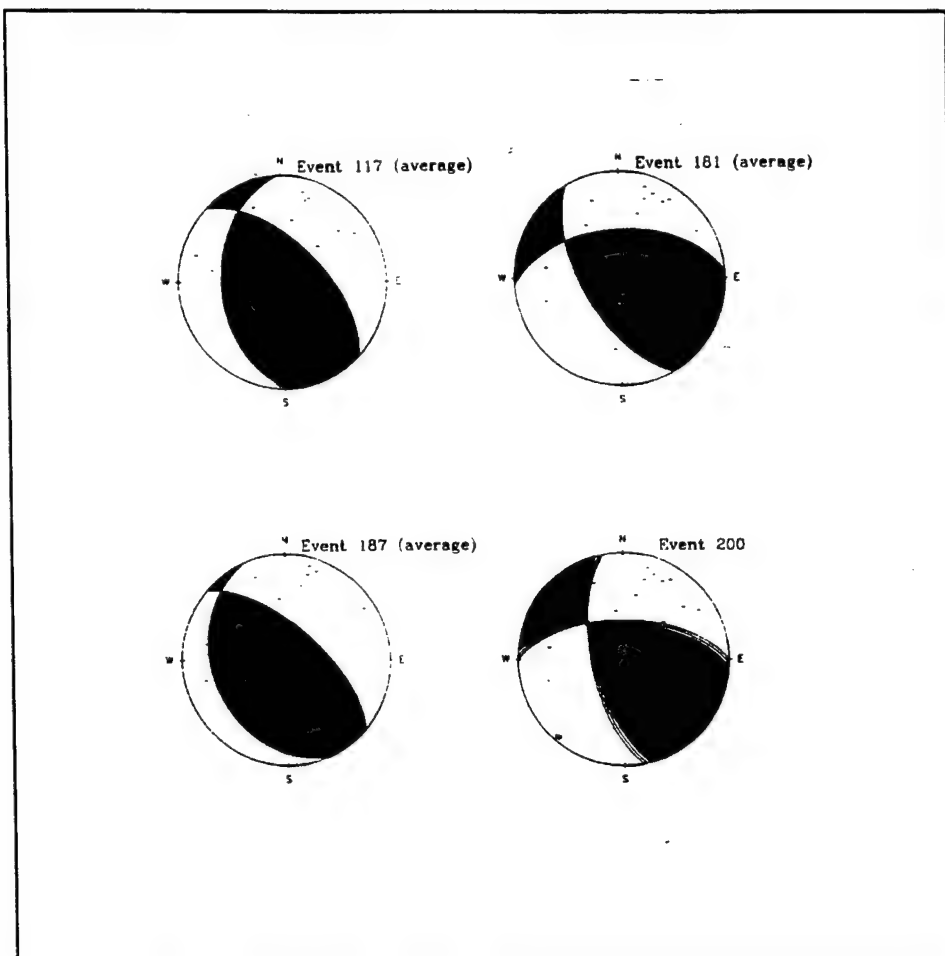
Figure 0-30: Focal mechanisms for four events. These examples are representative of the range of solutions found for seventeen events from the March 1993 cluster. Mechanisms for events 117, 181, and 187 are average solutions. where as the mechanism for event 200 are three solutions which fit the observed polarities for that event.

November 20. 1997 19:01

Figure 0-31: Epicentral locations of the event subset 157-187 in relation to depth contours fo the seismic "K" horizon and the sub-vertical discontinuities (countour map source ENEL, 1988).
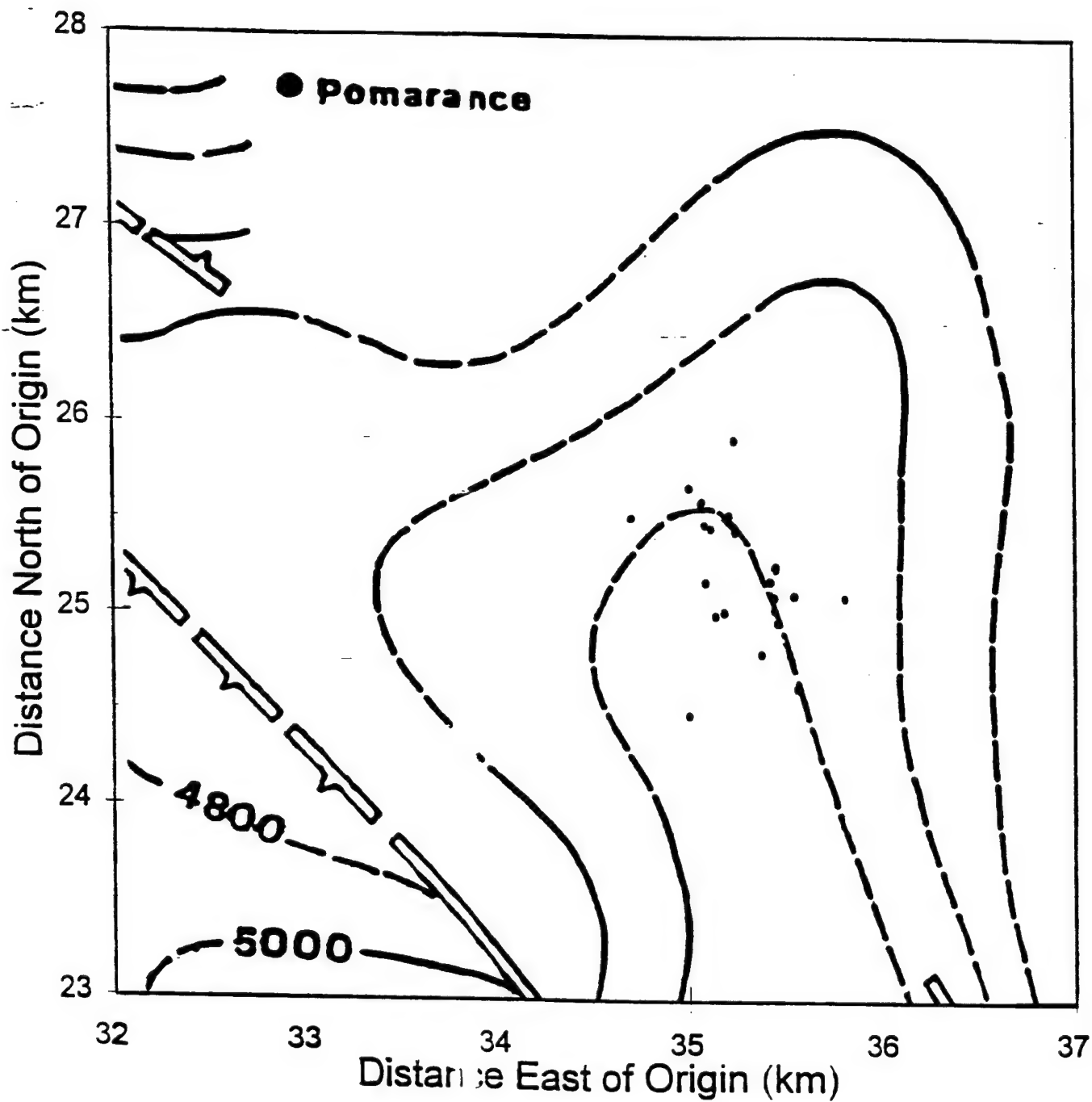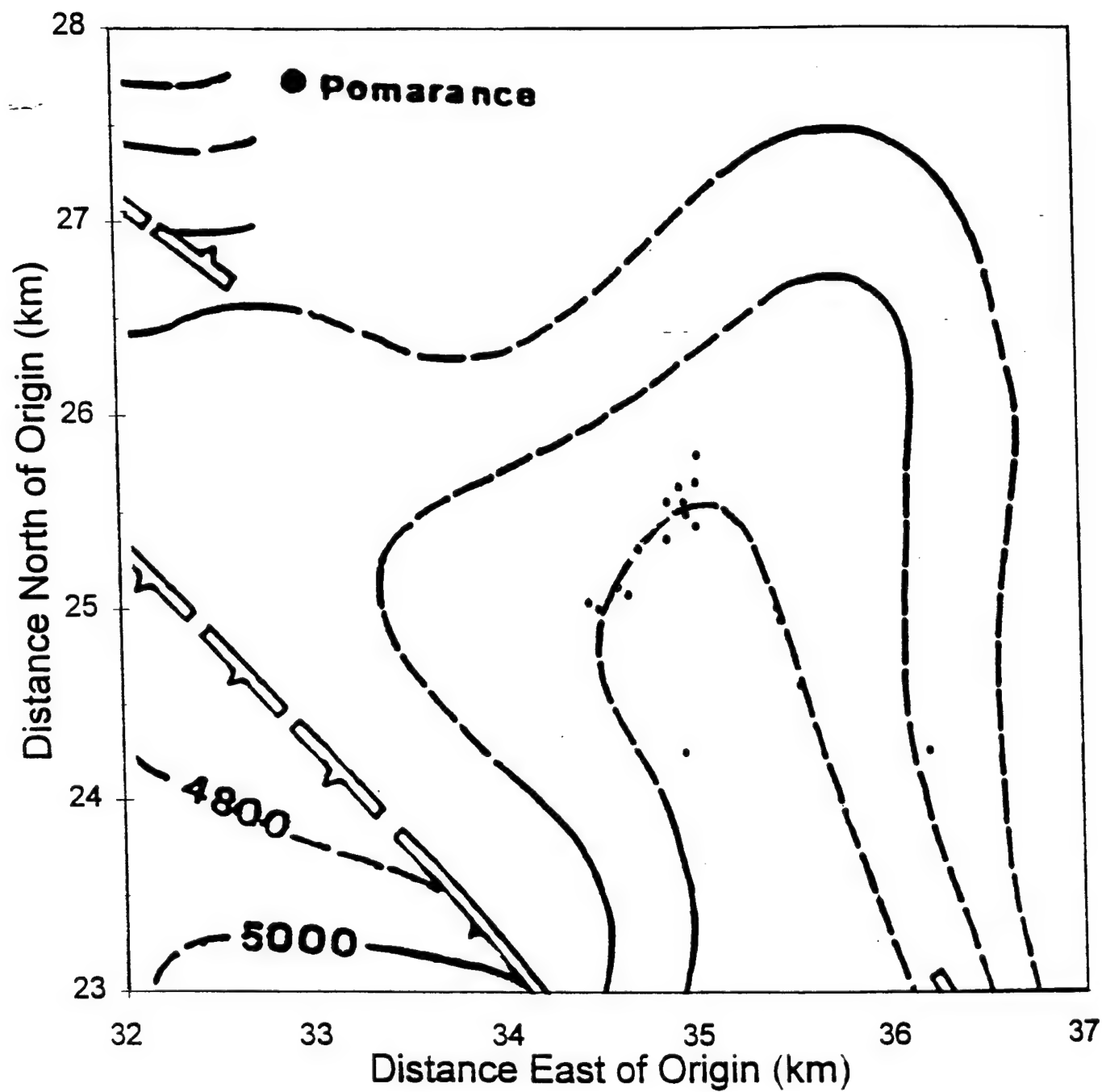
Figure 0-32: Epicentral locations of the event subset 188-218 in relation to depth contours fo the seismic "K" horizon and the sub-vertical discontinuities (countour map source EXEL. 1988).

Bibliography

Aki, K. and Richards, P. (1980). *Quantitative Seismology*, volume Volume I. W.H. Freeman and Company, New York.

Batini, F., Bertini, G., Gianelli, G., Pandeli, E., Puxeddu, M., and Villa, I. (191985b). Deep structure, age and evolution of the lardarello-travale geothermal field. In *Transactions of the Geothermal Resources Council*, volume 9-Part I. Geothermal Resources Council.

Batini, F., Duprat, A., and Nicolich, R. (1985a). Contribution of seismic reflection to the study of geothermal reservoirs in tuscany (italy). In *Transactions of the Geothermal Resources Council*, volume 9-Part I. Geothermal Resources Council.

Block, L. (1991). *Joint hypocenter-velocity inversion of local earthquake arrival time data in geothermal regions*. Ph.D. thesis, Massachusetts Institute of Technology.

Cameli, G., Dini, I., and Liotta, D. (1993). Upper crustal structure of the lardarello geothermal field as a feature of post-collisional extensional tectonics (southern tuscany, italy). Technical report, ENEL/V.D.A.G. and Dipartmento di Scienze della Terra, University di Siena, Siena, Italy.

Cappetti, G., Celati, R., Cigni, U., Squarci, P., Stefani, G., and Taffi, L. (1985). Developments of deep exploration in the geothermal areas of tuscany, italy. In *International Symposium on Geothermal Energy, International Volume*, volume 9-Part I. Geothermal Resources Council.

Carmignani, L. and Kligfield, R. (1990). Crustal extension in the northern appennine: The transition from compression to extension in the alpi apuane core complex. *Tectonics*, 9(6), 1275–1303.

Deichmann, N. and Garcia-Fernandez, M. (1992). Rupture geometry from high-precision relative hypocentre locations of microearthquake clusters. *Geophys. J. Int.*, pages 501–517.

ENEL-Unita Nazionale Geotermica (1988a). Isobate dell'orizzonte sismico K.

ENEL-Unita Nazionale Geotermica (1988b). Map of the Larderello-Travale geothermal field, top of the phyllitic formations.

ENEL-Unita Nazionale Geotermica (1988c). Structural map of the allocthonous flysch complex substratum, Larderello-Travale geothermal field.

ENEL-Unita Nazionale Geotermica (1993). Catalogo eventi elaborati. sequenza sismica de 20/3/93. File notes and catalog on magnetic media.

Flinn, E. (1965). Confidence regions and error determinations for seismic event location. *Reviews of Geophysics*, 3(1), 157–185.

Frankel, A. (1982). Precursers to a magnitude 4.8 earthquake in the virgin islands: spatial clustering of small earthquakes, anomalous focal mechanisms, and eathquake doublets. *Bulletin of the Seismological Society of America*, 72, 1277–1294.

Fremont, M. and Malone, S. (1987). High precision relative locations of earthquakes at Mount Saint Helens, Washington. *Journal of Geophysical Research*, 92, 10,223–10,236.

Geller, R. and Mueller, C. (1980). Four similar earthquakes in central California. *Geophysical Research Letters*, 7, 821–824.

Guinn, S. and Long, L. (1977). A computer methods for determination of valid focal mechanisms using p-wave first motions. *Earthquake Notes*, 48, 21–33.

Hartzell, S. (1978). Earthquakes aftershocks as green's functions. *Geophys. Res. Lett.*, 5, 1–4.

Hermann, R. (1975). A student's guide to the use of P and S wave data for focal mechanism determination. *Earthquake Notes*, **46**, 29–39.

Israelsson, I. (1990). Correlation of waveforms from closely spaced regional events. *Bull. Seism. Soc. Am.*, **80**(6), 2177–2193.

Ito, A. (1985). High resolution relative hypocenters of similar earthquakes by cross-spectral analysis method. *J. Phys. Earth*, **33**, 279–294.

Ito, A. (1990). Earthquake swarm activity revealed from high resolution relative hypocenters-clustering of microearthquakes. *Tectonophysics*, **175**, 47–66.

Jordan, T. and Sverdrup, K. (1981). Teleseismic location techniques and their application to earthquake clusters in the south-central Pacific. *Bulletin of the Seismological Society of America*, **71**, 1,105–1,130.

Li, Y., Rodi, W., and Toksöz, M. (1994). Seismic source characterization with empirical Green's function and relative location techniques. In *16th Annual PL/AFOSR Seismic Research Symposium*, Thornwood, New York.

Li, Y., Toksöz, M., and Rodi, W. (1995). Source time functions of nuclear explosions and earthquakes in central Asia determined using empirical Green's functions. *J. Geophys. Res.*, **100**, 659–674.

Li, Y., Toksöz, M., and Rodi, W. (1996). Discrimination of small earthquakes and explosions. In *18th Annual Seismic Research Symposium*, Anapolis, Maryland. Air Force Phillips Laboratory.

Menke, W. (1989). *Geophysical Data Analysis: Discrete Inverse Theory*, volume 45 of *International Geophysics Series*. Academic Press, Inc., San Diego, revised edition edition.

Minissale, A. (1991). The lardarello geothermal field: a review. *Earth-Science Reviews*, **31**, 133–151.

Mueller, C. (1985). Source pulse enhancement by deconvolution of an empirical Green's function. *Geophys. Res. Lett.*, **12**, 33–36.

Pechmann, J. and Thorbjarnardottir, B. (1990). Waveform analysis of two preshock-main shock-aftershock sequences in Utah. *Bulletin of the Seismological Society of America*, **80**, 519–550.

Phillips, W. S., House, L., and Fehler, M. (1992). Vp/Vs and the structure of microearthquake clusters. *Seismol. res. Lett.*, **63**, 56–57. Abstract.

Poupinet, G., Ellsworth, W., and Frechet, J. (1984). Monitoring velocity variations in the crust using earthquakes doublets: an application to the Calaveras Fault. *Journal of Geophysical Research*, **89**, 5,719–5,731.

Puxeddu, M. (1984). Structure and late cenozoic evolution of the upper lithosphere in southwest tuscany (italy). *Tectonophysics*, **101**, 357–382.

Puxeddu, M., Squarci, P., Rau, A., Tongiorgi, M., and Burgassi, P. (1977). Stratigraphic and tectonic study of the lardarello-travale basement rockes and its geothermal implications. *Geothermics*, **6**.

Riviere-Barbier, F. and Grant, L. (1991). Cluster analysis method applied to event location. In *Proceedings of the 13th Annual PL/DARPA Seismic Research Symposium*, pages 403–409, Keystone, Colorado.

Riviere-Barbier, F., Baumgardt, D., and Rodi, W. (1993). Using groups of similar events at the Scandinavian arrays to identify and lo locate events. In *Proceedings of the 15th Annual PL/ARPA Seismic Research Symposium*, pages 318–325, Vail, Colorado.

Rodi, W., Li, Y., and Cheng, C. (1993). Location of microearthquakes induced by hydraulic fracturing. In *Borehole Acoustics and Logging Consortium Annual Report*, pages 369–410. Massachussets Institute of Technology, Earth Resources Laboratory.

Rodi, W., Li, Y., and Toksöz, M. (1994). Research on monitoring at regional distances: multiple event location, final technical report. Technical report, Massachusetts Institute of Technology. Air Force Contract No. F29601-91-K-DB15.

Societa Elaborazione Cartographiche (1978a). Carta topografica regionale, regione Toscana. Quadrante 119-I.

Societa Elaborazione Cartographiche (1978b). Carta topografica regionale, regione Toscana. Quadrante 119-II.

Societa Elaborazione Cartographiche (1978c). Carta topografica regionale, regione Toscana. Quadrante 120-III.

Societa Elaborazione Cartographiche (1978d). Carta topografica regionale, regione Toscana. Quadrante 120-IV.

Thornjarnardottir, B. and Pechmann, J. (1987). Constraints on relative earthquake locations from cross-correlation of waveforms. *Bulletin of the Seismological Society of America*, **77**, 1,626–1,634.

Toksöz, M., Dainty, A., and Charrette, E. (1991a). Spatial variation of ground motion due to lateral heterogeneity. *Structural Safety*, **10**, 53–77.

Toksöz, M., Li, Y., and Rodi, W. (1993). Seismic source characterization with empirical green's function and relative location techniques. In *Proceedings of the 15th Annual PL/ARPA Seismic Research Symposium*, Vail, Colorado.

November 20, 1997 19:01